Realia et naturalia

DISSERTATIONES
PHYSICAE
UNIVERSITATIS
TARTUENSIS
93

SIIM PIKKER

Modification in the emission and spectral shape of photostable fluorophores by nanometallic structures

DISSERTATIONES PHYSICAE UNIVERSITATIS TARTUENSIS

93

DISSERTATIONES PHYSICAE UNIVERSITATIS TARTUENSIS
93

SIIM PIKKER

Modification in the emission and spectral shape of photostable fluorophores by nanometallic structures

UNIVERSITY OF TARTU
PRESS
1632

The study was carried out at the Institute of Physics, Faculty of Science and Technology, University of Tartu, Estonia.

The dissertation was admitted on June 19, 2014 in partial fulfilment of the requirements for the degree of Doctor of Philosophy (solid state physics), and allowed for defence by the Council of the Institute of Physics, University of Tartu.

Supervisors: Dr. Rünno Lõhmus, Institute of Physics, University of Tartu, Estonia;
Dr. Ilmo Sildos, Institute of Physics, University of Tartu, Estonia;
Dr. Leonid Dolgov, Institute of Physics, University of Tartu, Estonia.

Opponents: Professor Gintautas Tamulaitis, Head of Semiconductor Physics Department, Vilnius University, Lithuania.

Defence: August 21, 2014, University of Tartu (Tartu, Estonia)

This work has been partially supported by graduate school "Functional materials and technologies", receiving funding from the European Social Fund under project 1.2.0401.09-0079 in Estonia.

ISSN 1406-0647
ISBN 978-9949-32-633-4 (print)
ISBN 978-9949-32-634-1 (pdf)

University of Tartu Press
www.tyk.ee

TABLE OF CONTENTS

LIST OF ORIGINAL PUBLICATIONS INCLUDED IN THE THESIS

[1] S. Pikker, L. Dolgov, S. Heinsalu, S. Mamykin, V. Kiisk, S. Kopanchuk, R. Lõhmus, and I. Sildos, "Gilded nanoparticles for plasmonically enhanced fluorescence in TiO2:Sm3+ sol-gel films," *Nanoscale Res. Lett.*, vol. 9, no. 1, p. 143, 2014.

[2] L. Dolgov, V. Kiisk, R. Matt, S. Pikker, and I. Sildos, "Tailoring of the spectral–directional characteristics of rare-earth fluorescence by metal–dielectric planar structures," *Appl. Phys. B*, vol. 107, no. 3, pp. 749–753, May 2012.

[3] L. Dolgov, V. Reedo, V. Kiisk, S. Pikker, I. Sildos, and J. Kikas, "Structure and fluorescent properties of TiO2:Sm3+–Ag composite," *Opt. Mater. (Amst).*, vol. 32, no. 11, pp. 1540–1544, Sep. 2010.

[4] L. Dolgov, V. Kiisk, V. Reedo, S. Pikker, I. Sildos, and J. Kikas, "Sensitizing of Sm3+ fluorescence by silver dopant in the TiO2 films," *Cent. Eur. J. Phys.*, vol. 9, no. 2, pp. 542–546, Oct. 2010.

AUTHOR'S CONTRIBUTION

The following list contains detailed information about the contribution of the author of this thesis in the scientific papers on which the thesis is based. The author was involved in the planning of the experiments and the discussion of the results in all the included publications. The author's main contribution was in the discussion and theoretical analysis of the observed effects and his main task was to investigate the role of surface and localized surface plasmons in the observed phenomena.

The author of this thesis:

Paper 1: was responsible for the development of the experiments, the analysis of the prepared samples using electron microscopy and for the theoretical discussion about the role of localized surface plasmons in the observed phenomena. The author also participated in the preparation of the manuscript;

Paper 2: was responsible for the planning of the experiments, developing of the experimental measurement setup and was involved in the sample preparation. The author contributed to the theoretical calculations of the structures and to the discussion of the observed phenomena. The author also participated in the preparation of the manuscript;

Paper 3: was involved in the planning of the experiments and carried out the sample characterization with electron microscopy. The author also participated in the preparation of the manuscript and to the theoretical discussion of the role of localized surface plasmons in the observed phenomena;

Paper 4: was involved in the planning of the experiments and carried out the sample characterization with electron microscopy. The author also participated in the preparation of the manuscript and to the theoretical discussion of the role of localized surface plasmons in the observed phenomena.

LIST OF ABBREVIATIONS

Bg	Band-gap
LSP	Localized surface plasmon
CCD	Charge-coupled device
MEF	Metal enhanced fluorescence
SERS	Surface-enhanced Raman spectroscopy
SPCE	Surface plasmon-coupled emission
SPASER	Surface plasmon amplification by stimulated emission
SP	Surface plasmon
SPR	Surface plasmon resonance
RE	Rare-earth
RT	Room temperature

1. INTRODUCTION

The optically generated collective electron density waves on metal-dielectric boundaries known as surface plasmon polaritons or simply surface plasmons have been of great scientific interest since their discovery [1]–[6]. Being electromagnetic waves themselves, surface plasmons and localized surface plasmons (SP-s localized on small metallic features) interact strongly with light and give rise to the vibrant colours in gold and silver colloids. This effect is caused by the strong absorption and scattering of light on plasmonic particles [1]–[3], [6]–[9]. Resonant generation of SP waves can give rise to very high electric fields in the vicinity of the evanescent plasmon waves. These strong electric fields near the metal surfaces have been used in novel applications like surface enhanced Raman spectroscopy [10]–[16], metal enhanced and surface plasmon-coupled fluorescence [17]–[25], plasmonic lithography [26], plasmonic trapping of particles [27]–[32] and plasmonic light trapping inside solar cells [33]–[36] etc. Resonant coupling of surface plasmons to fluorescent emitters can strongly modify the emitted intensity, the angular distribution and the polarization of the emitted radiation and even the spontaneous radiative decay times of the luminescent emitters [17], [19], [23], [25]. The phenomenon of radiative lifetime shortening is most intriguing as it causes enhanced emission and increased photostability of fluorophores and possesses therefore high practical value [6], [17]–[23]. More exotic applications of plasmon coupled emission are the loss compensation of surface plasmon waveguides, SPASER-s, plasmon assisted lasing, single molecule fluorescence measurements, SPCE in biological sensing, optical qbit designs etc. [37]–[45]. Plasmonics is an exponentially growing research field and so it is understandable that also the number of different applications is exponentially growing. The subject of the present thesis is related to the spectroscopic study of the plasmon coupled photostable emitters. Fluorescent emitters have long been of enormous scientific and practical importance with applications in various scientific disciplines and in everyday life e.g.in lighting and display technologies. There exists also a growing need for new stable, brighter and more efficient fluorescent emitters and devices as traditionally used fluorescent organic molecules tend to suffer of strong photo-bleaching behaviour and are sometimes accompanied by unwanted photoblinking. In this thesis a study of plasmonically coupled photostable rare earth dopant containing inorganic matrices and fluorescent nitrogen vacancies in nanodiamond hosts is presented. These fluorescent systems exhibit unique physical properties and are therefore of high scientific importance. The main goal of this work is to investigate the optical effects induced by plasmonic structures, which interact with the fluorescent systems.

2. LITTERATURE OVERVIEW AND THEORETICAL BACKGROUND

2.1. Peculiarities of selected fluorophores

2.1.1. Fluorescence of rare earth impurity centres

Rare earth elements, presented in Table 1, can form stable compounds with partially filled electronic shells, which give them unique optical properties. These partially filled d and f shells can undergo spectrally narrow electronic transitions and cover a spectral range from the vacuum-ultraviolet to the far-infrared. These narrow optically active transitions are the basis for a whole range of practical applications as they cover also the visible spectrum. In rare earth compounds the 4f electrons are localized near the ion and they are also "shielded" by fully occupied shells by 5s and 5p electrons. In rare earths the lowest energy 4f electrons are spatially not the outermost ones. This unique feature is the cause of the rare earths atom like narrow spectral lines as they interact with the host matrix only weakly. The transparent host matrixes implanted with trivalent rare-earth impurities are of great potential in the fields of laser gain media, luminescent materials and in waveguide and sensorics applications [46].

Table 1. List of rare earth elements containing also yttrium which has similar chemical properties.

Element	**Symbol**	**Atomic number**
Yttrium	Y	39
Lanthanum	La	57
Cerium	Ce	58
Praseodymium	Pr	59
Neodymium	Nd	60
Promethium	Pm	61
Samarium	Sm	62
Europium	Eu	63
Gadolinium	Gd	64
Terbium	Tb	65
Dysprosium	Dy	66
Holmium	Ho	67
Erbium	Er	68
Thulium	Tm	69
Ytterbium	Yb	70
Lutetium	Ly	71

In the present study we investigate predominantly the Sm^{3+} doped TiO_2 system and analyse the modification of the radiative properties by plasmonic silver nanoparticles, smooth gold films and core-shell nanoparticles [47]–[51]. For understanding the fluorescent systems involved, the energy scheme of Sm^{3+} doped TiO_2 system is presented. In Figure 1 the high-resolution low-temperature (10 K) photoluminescence spectra of Sm^{3+} doped TiO_2 with anatase and rutile structure are given [52].

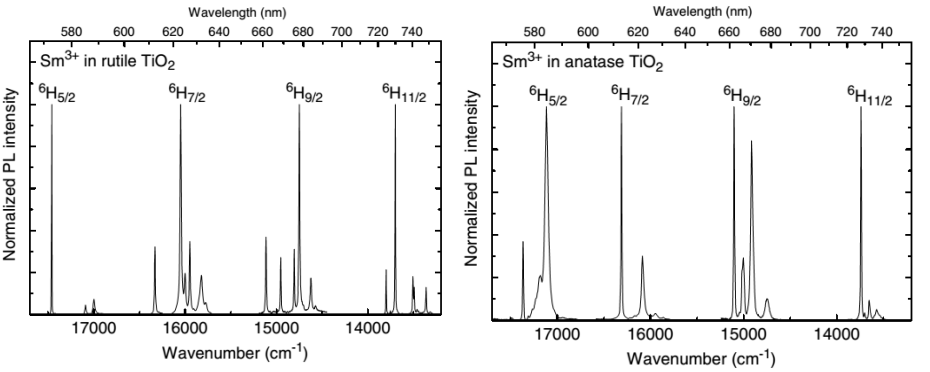

Figure 1. Normalized high-resolution photoluminescence spectra of Sm^{3+} in rutile and anatase phases recorded at 10 K and λ_{ex} = 355 nm [52].

2.1.2. Fluorescence of nitrogen vacancies in nanodiamonds

Defect free pure diamond is a wide band-gap semiconductor (with Bg = 5.5 eV) and is colourless in the visible spectrum. However, defects and incorporated impurity ions can form more than 500 identified colour centres. Diamond is known to form optically active centres with many enclosed chemical elements, including Ag, As, B, Co, Cr, H, He, Li, N, Ne, Ni, O, P, Si, Zn, Zr, Ti, Tl, W and Xe [53], [54]. In the entire list of colour centres, nitrogen impurities have probably gained the most scientific interest. Although nitrogen can form different complexes in diamond, two of the most important and most studied fluorescent complexes are the charge neutral nitrogen vacancy complex NV^0 and the negatively charged nitrogen vacancy complex NV^-. The NV^- state has been under intense scientific interest, because of its unique electronic structure, which enables room temperature control over its spin states, it has a long spin coherence time and it is suitable for a single photon emission. These properties make the NV^- complex an extraordinary research subject for quantum computing experiments [53]–[55].

Figure 2 A shows the excitation spectra of the NV^0 and NV^- complexes. The NV^- complex produces a strong purely electronic transition line at 637 nm (1.945 eV), which is the zero phonon line (ZPL). The ZPL is associated with the dipole transition between the electronic ground state $^3A_2$ and the excited state ^3E [54]. The NV^0 complex has a strong ZPL at 575 nm (2.156 eV). This transition

has been assigned to the transition between the ground state ^2E and the excited state $^2A_1$ [54]. The zero phonon lines of the NV^0 and NV^- complexes are both accompanied with observable phonon sidebands in the excitation and emission spectra. Figure 2 B shows the room temperature fluorescence spectra of nitrogen containing diamond film and exhibits both ZPL-s. Normally both charge states exist in the same sample. Both states can be present also in small nanoparticle samples and there exist a number of recent reports of photochromic switching between the NV^0 and NV^- charge states [56]–[59].

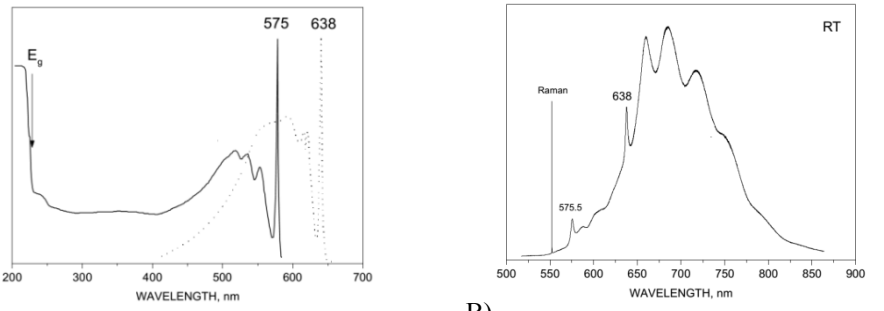

A) B)

Figure 2. The excitation (a) and photoluminescence (b) spectra of the NV^0 and NV^- complexes [53].

2.2. Fundamental principles plasmonic enhancement of emission

2.2.1. Metal enhanced fluorescence

Fluorescence is a luminescence process, where a light induced excitation within a substance will decay via emission of light. It is also called photoluminescence. Fluorescence is the light emission and electronic relaxation from an excited singlet electronic state and differs from phosphorescence, where the excited state is a triplet [17], [25], [37]. The process of fluorescence (the absorption and emission of light with some intermediate energy transfer and loss mechanisms) can be described by the Jabłoński diagram formalism. Figure 3 shows a simplified Jabłoński diagram with the processes involved in the fluorescence phenomena.

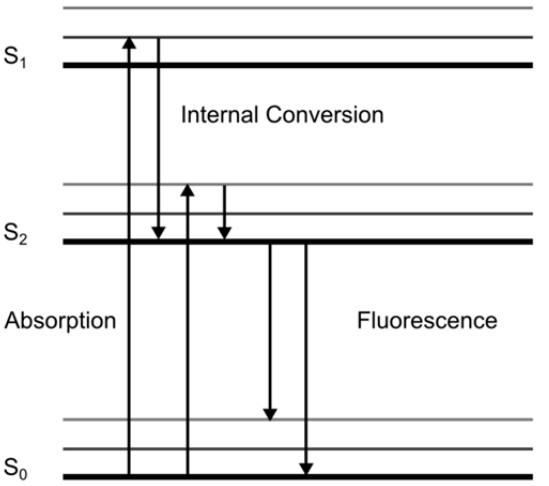

Figure 3. A simplified Jabłoński showing the mechanisms involved in the fluorescence process [17].

The different stages involved in the light energy absorption, transformation and emission are described by rate equations. The fluorescence and internal conversion processes are also described by the internal conversion lifetime τ_{ic} and the fluorescence lifetime τ_f. The fluorescence lifetime is defined as the average relaxation time from the excited electronic site to the electronic ground state. The typical lifetimes for fluorescence in molecules are in the order of nanoseconds and the internal conversion times are in the picosecond scale. The overall fluorescence quantum yield can be used to describe an emitter's efficiency for radiative decay. The fluorescence quantum yield is defined by the ratio of the number of emitted photons to the number of absorbed photons. Three equivalent equations for the calculation of fluorescence quantum yield for an isolated emitter are given with eq 1, 2 and 3,

$$\phi_f = \frac{N_{em}}{N_{abs}} \tag{1}$$

$$\phi_f = \frac{k_{f,r}}{k_{f,r}+k_{f,nr}} \tag{2}$$

$$\phi_f = \frac{\tau_{f,nr}}{\tau_{f,nr}+\tau_{f,r}} \tag{3}$$

In these equations ϕ_f is the fluorescence quantum yield of the excited emitter, N_{em} is the number of emitted photons, N_{abs} is the number of absorbed photons, $k_{f,r}$ and $k_{f,nr}$ are the intrinsic radiative and non-radiative decay rates of the

excited electronic state in the units of s^{-1} for a free emitter and $\tau_{f,r}$ and $\tau_{f,nr}$ are the radiative and nonradiative decay times of relaxation processes for the fluorophore [17], [19], [23], [25], [37], [41].

The overall fluorescence intensity I of a fluorescent emitter can be expressed by

$$I = k_{ex} \cdot \phi_f \cdot \varepsilon_{col} \,, \tag{4}$$

where k_{ex} denotes the excitation rate of the emitter, ϕ_f is the fluorescence quantum yield and ε_{col} denotes the system-dependent light collection efficiency of the optical measurement setup. The excitation rate is given by Fermi´s golden rule and is a function of the local electric field $\boldsymbol{E}$, given by

$$k_{ex} = (4\pi^2/h) \cdot |\langle e|\boldsymbol{E} \cdot \boldsymbol{p}|g\rangle|^2 \, \rho_e \,, \tag{5}$$

where h denotes the Planck´s constant and e and g are the excited state and ground state wavefunctions, respectively. Included also in this equation are $\boldsymbol{p}$ that denotes the absorption transition dipole momentum and ρ_e which stands for the density of the excited state [25].

In the vicinity of metal nanostructures the overall fluorescence of the emitter will be changed as the metal structures can modify all of the three variables of the fluorescence intensity. Metallic structures, that support SP-s or LSP-s can localize and enhance the local electric field strength and thereby enhance the excitation rate of the emitter. The metal structures can also modify the spatial distribution properties of the fluorescence, which can result in the modification of the light collection efficiency. Metal structures (nanoparticles, nanostructures and thin films) can also change the radiative decay times through the modification of the local density of states for the electromagnetic interaction [37], [60], [61]. In a simplified model one can think of this phenomenon as a generation of extra decay channels which are formed in the vicinity of metal structures.

A free excited fluorescent emitter without the nearby metal surface has the possibility for radiative or non-radiative decay. The addition of a metal surface generates two extra decay paths. Therefore, channels for metal mediated radiative relaxation and for metal mediated non-radiative decay are created [19], [23], [25], [41]. The metal modified system also has now an altered overall fluorescence quantum yield, which is given by

$$\phi'_{fm} = \frac{k_{f,r}+k_{fm,r}}{k_{f,r}+k_{fm,r}+k_{f,nr}+k_{fm,nr}}. \tag{6}$$

In equation 6 ϕ'_{fm} denotes the metal modified overall fluorescence quantum yield of the fluorophore-metal system, $k_{fm,r}$ and $k_{fm,nr}$ are the metal mediated

radiative and non-radiative decay rates of the fluorophore. The modified overall quantum yield has now extra parameters, which can now, depending on their values, increase or decrease the overall quantum yield.

There exists an alternative definition of the modified overall quantum yield, that is closely related to equation (6), which was given by [37] and gives extra physical insight to the processes involved. When changing the local environment of the fluorophore, we change the overall quantum yield of the system to

$$\phi'_{fm} = \frac{k_r}{k_r + k_{f,nr} + k_{abs} + k_m} \tag{7}$$

Here ϕ'_{fm} also denotes the metal modified overall fluorescence quantum yield, k_r has here a modified meaning compared to $k_{f,r}$ and is now the radiative rate of the coupled system and not just the intrinsic radiative rate of the emitter in free space. The $k_{f,nr}$ still denotes the intrinsic non-radiative decay rate for the free emitter. The two new parameters k_{abs} and k_m account for the dissipated heat and non-radiative electromagnetic modes, respectively [37].

It has been shown, that the metal mediated radiative and non-radiative decay rates are in strong dependence of the fluorophore metal distance. Emitters very close (ca <10 nm) from the metals surface tend to be quenched as the energy transfer from the emitter to the metal surface at these length-scales is preferentially non-radiative and the energy is coupled to phonons, surface phonon polaritons, surface plasmon polaritons and the energy is also dissipated as heat [2], [17], [19], [20], [25], [37], [62]–[64]. When the emitter is placed near a metal or dielectric surface strong coupling to non-radiative electromagnetic modes also called the forbidden light domain can be achieved. This light is normally lost and is not usually available for measurement and imaging techniques. But by using special out-coupling methods one can convert these non-radiative electromagnetic modes to far-field radiation. The most known and implemented methods for such near-field out-coupling are the total internal reflection fluorescence (TIRF) microscopy [65], [66], supercritical angle fluorescence (SAF) microscopy [67], [68] for dielectric surfaces and surface plasmon fluorescence spectroscopy (SPFS) [69], SPP enhanced TIRF microscopy for metal surfaces [70].

Coupling of the fluorescence of emitters to surface plasmons takes most effectively place in the distance range of 10–100 nm and has been reported to be most efficient at ca 20 nm [17], [19], [23], [25], [37], [71]. To supress energy dissipation to heat and other non-radiative processes usually a thin (ca 5–10 nm thick) dielectric spacer layer is used in fluorescence enhancing experiments.

If we now consider the overall florescence intensity of a fluorescent emitter near a metal nanoparticle, then various effects have to be considered. The summed up effects to the overall fluorescence intensity are then as follows. The enhanced near-fields near a resonantly excited particle result in enhanced

excitation rate of the emitter. In the presence of a metal nanoparticle or structure we have a modified optical mode density and extra relaxation channels for the decay of the excited states of the emitter. If the emitter decays through plasmon excitation, then the radiative and non-radiative decay of the plasmons has to be accounted for. For a nanoparticle, this can be achieved if we introduce the wavelength dependent scattering cross-section (C_{scat}) and the wavelength dependent absorption cross-section (C_{abs}) of the nanoparticle. If we now neglect the modifications to the system-dependent light collection efficiency of the optical measurement setup, we get a modified equation of the overall fluorescence intensity near a metal particle, which is as follows [25]:

$$I' = k'_{ex} \cdot \left(\frac{k_R}{k_R + k_{NR} + k_{ET}} + \frac{k_{ET}}{k_R + k_{NR} + k_{ET}} \cdot \frac{C_{scat}}{C_{scat} + C_{abs}} \right) \cdot \varepsilon_{col} \quad (8)$$

k'_{ex} denotes here the modified excitation rate, which has been changed by the local electric field near the nanoparticle. k_R is now the modified radiative decay rate of the emitter, which does not account for the metal mediated radiative decay, k_{NR} denotes here the non-radiative decay channel, which does not account for the energy lost in the nanoparticle and k_{ET} denotes the energy transfer rate from the excited emitter to the metal nanoparticle. The proportion of the energy which will be scattered as light by the nanoparticle and is also accountable in the overall fluorescence intensity, can be characterized by the values of the scattering cross-section C_{scat} and absorption cross-section C_{abs} [25].

2.2.2. Surface plasmon-coupled emission (SPCE)

Surface plasmon-coupled emission is the process, where an emitter in close proximity (~10–200 nm) to a metal structure supporting plasmon modes is electromagnetically coupled to the radiatively decaying plasmon modes. SPCE process was first described on smooth continuous thin (~50 nm) silver and gold films by Lakowicz et al. and is related to the surface plasmon resonance (SPR) effect [20], [22], [38], [72]. The SPCE is considered a reversed SPR process because the coupled emitters excite surface plasmons, which can radiate to the wavelength dependent SPR angles in the Kretschmann scheme [1], [2], [20], [22], [38], [72], [73]. The geometry of the Kretschmann SPR excitation scheme is depicted in Figure 4 A.

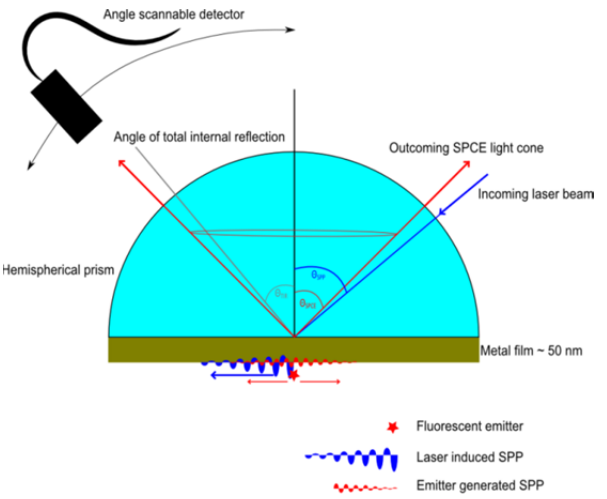

A.

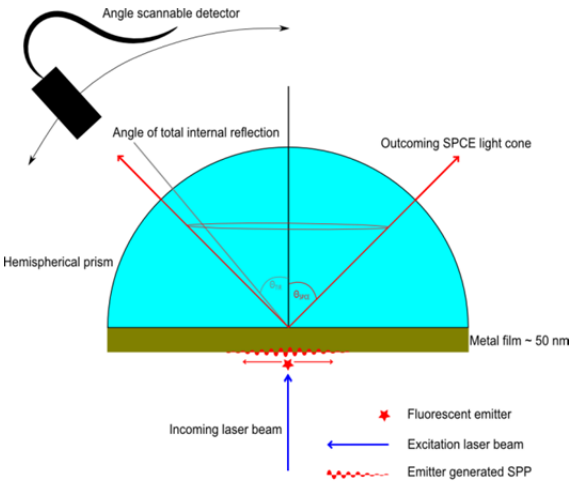

B.

Figure 4. A. Kretschmann excitation scheme for SPCE experiments. The fluorescent emitters are excited by the evanescent fields generated by laser induced surface plasmon polaritons. The SPP-s are generated by a p-polarized laser beam incident from the prism. The angle for SPP generation is the usual surface plasmon resonance angle, which is determined by the wavelength and the wavelength dependent dielectric properties of the prism, metal and the dielectric medium on the fluorophore side of the metal. B. The reversed Kretschmann geometry for SPCE experiments. Here the incident laser excites directly the fluorescent emitter, which then induces SPP-s in the metal film. These SPPs have an energy spectrum, which closely resembles the emitter's fluorescence spectrum. The induced surface plasmon can decay as leakage radiation through the prism as a radially polarized light cone. The angle of cone is wavelength dependent and the maximum intensity is close to the SPR angle for that wavelength.

In the Kretschmann geometry one uses a prism to couple the light to surface plasmons. The prism is covered with a thin ca. 50 nm Ag or Au film which can support surface plasmons. One uses a prism with a higher refractive index than the medium which is in contact with the other metal film boundary to satisfy the wave-vector matching condition known from conventional SPR experiments. In the Kretschmann setup the incoming laser beam is p-polarized and it is coupled through the prism at a wavelength dependent SPR angle to resonantly excite a surface plasmon mode. The excited surface plasmons excite the fluorescent emitters via the generated evanescent field. The nearby fluorescent emitters will then excite surface plasmon modes in the metal field. These emitter induced surface plasmons can radiatively decay through the prism as light. This special light is called surface plasmon-coupled emission. The unique properties of this type of emission are that the light is strongly p-polarized (radially polarized for the whole light cone) and it has the spectral composition of the fluorescent emitters, which induced the surface plasmons. The out-coupled light has also a wavelength dependent angular distribution, and the maximal intensity of the emitted light at a certain wavelength corresponds to the SPR angle for this wavelength. These mentioned properties considerably aid the experimental identification of the SPCE effect and helps to distinguish SPCE from waveguide modes if the studied samples are for example fluorescent dielectric films.

One alternative SPCE excitation scheme is the reversed Kretschmann scheme in which the fluorescent emitters are directly excited by a laser beam. The excited emitters in the proper distance from the metal film (~10–200 nm) decay by excitation of surface plasmons, which out-couple through the prism. The resulting emission is like in the Kretschmann scheme p-polarized and forms a light-cone with an angular distribution, which depends on the spectrum of the emitter. The reversed Kretschmann scheme is depicted in Figure 4 B.

SPCE is a surface sensitive technique because the metal mediated decay of the excited fluorescent emitters through the excitation of surface plasmon is a distance dependent phenomenon. This surface sensitivity and polarisation dependence has been used in various biological sensing and high contrast and background suppression imaging applications [19], [20], [22], [38], [39], [41], [70]. It is also possible to combine the Kretschmann and reversed Kretschmann SPCE experimental setups with the Fourier plane imaging technique under oil immersion microscopes giving rise to a new microscopic method called leakage radiation microscopy (LRM) [74]–[76]. This microscopic technique allows direct imaging of the leakage radiation produced by radiative decay of surface plasmons and is used as a tool to study dielectric loaded plasmonic waveguides and it is also suitable for plasmonic loss compensation experiments.

2.2.3. Fluorescence enhancing plasmonic substrates and systems

The research of high efficiency fluorescence systems has given already a myriad of plasmonic substrates and systems, which can be constructed to enhance the properties of the emitted fluorescence. The classical plasmonic substrates for enhanced fluorescence experiments range from simple evaporated silver or gold films [63], [69], [77], single nanoparticles [62], single crystal nanowires [78], self-organizing nanoparticle films (fabricated with the thermal dewetting process [79]) also called the silver or gold island films [23], structures obtained with colloidal lithography , different kind of metallic nanoantenna geometries fabricated with electron beam lithography [80], even more complicated systems fabricated with focused ion beam setups and the list goes still on. In the pioneering works of Drexhage et al. simple thick film metallic mirror surfaces were used for the measurement of modification of the emitter's fluorescence properties. Amos and Barnes (in 1997) used a similar simple system to investigate the modification of the spontaneous emission rate of Eu^{3+} ions in chelate host Langmuir-Blodgett film systems and characterized the distance dependent lifetime modification and presented data, which show the decay of the excited emitters into SPP relaxation channel on thin metal films. Lakowicz developed the substrates further and used silver-island-films and continuous smooth film systems enhanced with coupled metal nanoparticles to further enhance the fluorescent properties of emitters. Single nanoparticles, and coupled nanoparticles have been used to enhance the excitation rate and radiative-decay rates amounting for enhanced fluorescence intensities. Bowtie antennas and electromagnetically coupled spherical and cylindrical nanoparticles are extensively studied as also the reported metallic nanohole arrays.

A recent report of the application of a commercially available micro and nano-structured SERS substrate (Klarite, depicted in Figure 5), to enhance the fluorescence of molecules placed on top of it motivated us to employ these substrates in the characterization of plasmon coupled fluorescence of photostable NV-centres in fluorescent nanodiamonds [81].

The present study focused predominantly on the plasmonic enhancement of rare-earth ions incorporated into metal oxide hosts, which were prepared using sol-gel techniques and the plasmonic systems were chosen to be compatible with these techniques. The emphasis was on continuous thin film samples, which were doped with metal nanoparticles and insulator-metal-insulator samples in which a smooth thin gold film was covered by a thin layer of rare-earth containing metal oxide. Rare-earth doped metal oxide films, which were modified by incorporating plasmonic core-shell nanoparticles, were also investigated.

3. GOALS OF THE STUDY

For any practical implementation of sophisticated physical phenomena one needs to understand underlying physics and the basic behaviour of the systems where the phenomena exist. Plasmon-fluorophore coupled systems are therefore no exception. The present study is an experimental investigation of the fluorescence behaviour of high refractive index photostable fluorophore materials with enclosed or nearby plasmonic structures. Most of the scientific community investigating plasmonic interactions with fluorophores consider predominantly only low-refractive index media (mostly polymers and solutions), which have been doped with organic dye molecules. These systems are quite easy to manufacture, but are prone to photo bleaching which obstruct the implementation of these systems in real applications. The fluorescent media, which are studied in this thesis, are of great scientific and practical importance as they do not suffer under photo bleaching, have high quantum yields and demonstrate other unique physical properties. The photostable RE doped oxides possess very narrow band emission spectra which is of great practical importance to labelling, sensing, lasing and light conversion applications. The NV-centres in nanodiamonds are also of great interest as they exhibits strong room temperature ZPL lines and shows a rare type of spin behaviour, which can lead to their application in quantum computing. Plasmonic structures enable the focusing of light energy to sub-diffraction limited volumes, can be used for waveguiding in miniature devices and allow the enhancement of fluorescence. These are but a few applications of plasmonic waves but they are also the main reasons why it is of great practical importance to understand the effects induced by these metallic structures to the emission properties of these fluorescent materials.

The experimental investigation presented in this work specifically aims to determine the phenomena induced by the metallic structures to the fluorescence of the described materials. To accomplish the task the work has the following specific goals:

1. To incorporate plasmonic particles into RE doped oxide materials fabricated by the sol-gel method and to investigate the emission and structural properties of such composite materials and to determine the role of plasmonic phenomena.
2. To fabricate planar dielectric-metal-dielectric structures for SPCE experiments with high refractive index fluorescence RE doped oxide films and for the narrow band study of the SPCE phenomenon and possible waveguiding effects. And to characterize the angular and polarization dependence of the coupled emission of such structures.
3. To investigate possible spectral modifications of fluorescent nanodiamonds induced by nearby plasmonic structures.

4. EXPERIMENTAL METHODS

4.1. Sample preparation and characterization

In the current work, three general types of different fluorophore systems were studied. First type of nanostructures that were investigated consisted of rare earth ion doped metal oxide thin films, which contained plasmonic particles. The second types of samples were RE doped oxide thin films on thin metallic films suitable for SPCE experiments. Both the metal films and the nanoparticles incorporated into the oxide films were chosen to support surface or localized plasmon waves. The third type of fluorophore systems were NV complex containing fluorescent nanodiamonds, which were placed on a commercially available nanostructured gold substrate, which supports plasmon waves and are used in surface enhanced Raman spectroscopy.

4.1.1. Sol-gel derived rare earth doped oxides

The exact procedures of the fabrication of rare-earth ion doped metal oxide samples are described in detail in the referred articles included in the thesis. Here I describe only the fundamental fabrication technique of the sol-gel process used for the production fluorescent rare-earth doped metal oxides.

Host titanium dioxide was prepared by sol-gel method with hydrolysis and polycondensation of $Ti(OBu)_4$ (Alfa Aesar, 98 wt %). The precursor was obtained after mixing of distilled water and n-butanol (YA-KEMIA OY) with $Ti(OBu)_4$ (mole ratio 1:24:1.6) and subsequent stirring for 1 h at 21°C. This was followed by incorporation of commercially available Ag nanoparticles (Nanoamor) or the silica-gold core-shell nanoparticles fabricated by us. The next step involved the doping of the nanoparticle containing precursor with samarium salt $Sm(NO_3)_2 \cdot H_2O$ (1 mol % or 2 wt % relatively to the weight of the TiO_2 film). For the SPCE experiments the same sol-gel solution without metal nanoparticles was spin coated on top of a metal thin film substrate.

4.1.2. Fluorescent nanodiamonds with nitrogen vacancies

Investigations of the plasmon modified emission of fluorescent NV centre containing nanodiamonds were done using commercially available fluorescent nanodiamonds (FND) with the size of 140 nm. The nanodiamonds were purchased from from Adamas Nanotechnologies Inc. (USA). The FNDs had a diameter of 140 nm. The FNDs were drop and spin coated onto a commercially available micro- and nanostructured KLARITE 303 surface enhanced Raman spectroscopy (SERS) substrates. The substrates consist of lithographically structured Si wafer, which was covered with a roughened Au film. The structures consist of ordered inverted pyramidal features as depicted in Figure 5.

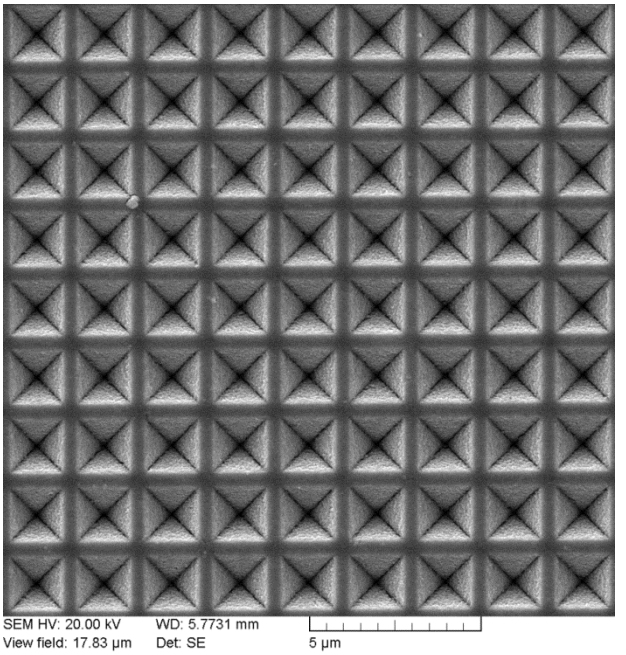

Figure 5. A scanning electron micrograph of the nano- and micro-structured KLARITE 303 SERS substrate used in the plasmon-coupled emission experiments with NV centres in nanodiamonds.

It was found that the traditional spin coating technique was more suitable for the placement of FNDs into the pyramidal microstructures. The slow drying process with the simple drop coating method was not suitable for the placement of the FNDs into the cavities of the structure, because the self-organisation of the FNDs when using the slow drop coating method resulted in that most of the FNDs were placed in the areas between the resonant cavities. It is believed, that the relative big size of the nanoparticles is the reason why it is difficult to place the FNDs inside the voids, as they tend to get pinned at surface with relatively high roughness.

4.2. Experimental measurement setup

The measurement system for the SPCE thin film experiments consisted of a BK7 glass semi-cylindrical coupling prism mounted on a simple manual rotational stage and a commercial photodiode or a fibre coupled spectrometer mounted on another rotational stage. The system was further developed in the later stages of the experiments and consists now of a computer controlled automated rotational stages for the variable angle excitation and measurement of the SPCE light. More exact description for the measurement setups used can be found in the included articles.

5. RESULTS AND DISCUSSION

5.1. Enhanced fluorescence in RE doped metal oxides by incorporated silver nanoparticles

The fluorescence of the Sm^{3+} ions in TiO_2 host matrix was modified by the introduction of Ag nanoparticles to the system. Silver nanoparticles with the primary particle size of 30–50 nm were introduced to the host during the sol-gel fabrication procedure. The main aim of incorporation of silver nanoparticles was to observe metal induced modifications of samarium ion fluorescence. In [49], [50] it was found, that the Ag nanoparticles incorporated into the TiO_2 host matrix did modify the fluorescence intensity. Comparative measurements of fluorescence intensities were carried out with three different excitation schemes. The direct excitation scheme uses direct excitation of the f-f transition of rare-earth ions with the excitation wavelength of 488 nm. The indirect excitation scheme with the excitation wavelength at 355 nm is used to pump the TiO_2 host with the following non-radiative energy transfer from the host to the Sm^{3+} ions. The indirect excitation of the Sm^{3+} ions is known to be more efficient as the effective cross section for the indirect excitation is several orders of magnitude higher than for the direct excitation [82]. The incorporated silver nanoparticles had a plasmonic resonance wavelength at around 400 nm, which was determined using transmission spectroscopy and shown in Figure 6 [49]–[51]. An excitation wavelength of 410 nm was also used, to enhance the fluorescence emission through resonant localized surface plasmons pumping the system.

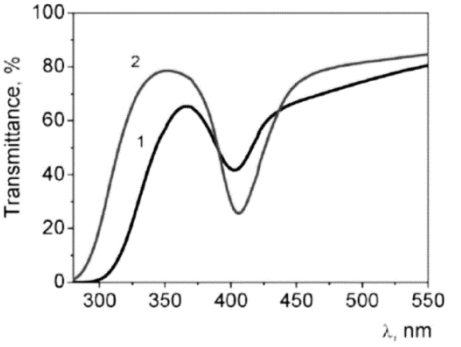

Figure 6. Transmission spectra of the prepared metal oxide films with incorporated silver nanoparticles: (1) TiO_2doped with 4 wt. % of silver nanoparticles (30–50 nm); (2) ZrO_2 doped with 8 wt. % of silver nanoparticles (5–15 nm). The substrate material was glass in both samples. [51]

The excitation wavelengths for both the direct and indirect excitations are off the plasmonic resonance wavelength. This means that no strong enhancement effects were expected due to enhanced absorption and higher local electric

fields. The plasmonic resonance at 400 nm differs substantially also from the emission bands of Sm^{3+} ions shown in Figure 1. It was then expected that there will be no significant modifications of the fluorescence intensities. Just the opposite was found in the experiments. We found that silver nanoparticles dispersed in the samarium doped TiO_2 films did give rise to enhanced fluorescence intensities even without the direct involvement of localized surface plasmons in the absorption or emission process. The fluorescence spectra at the different excitation wavelengths displayed similar structure at the broad scale, but the finer features in the photoluminescence spectra varied considerably with the excitation wavelength (see Figure 7).

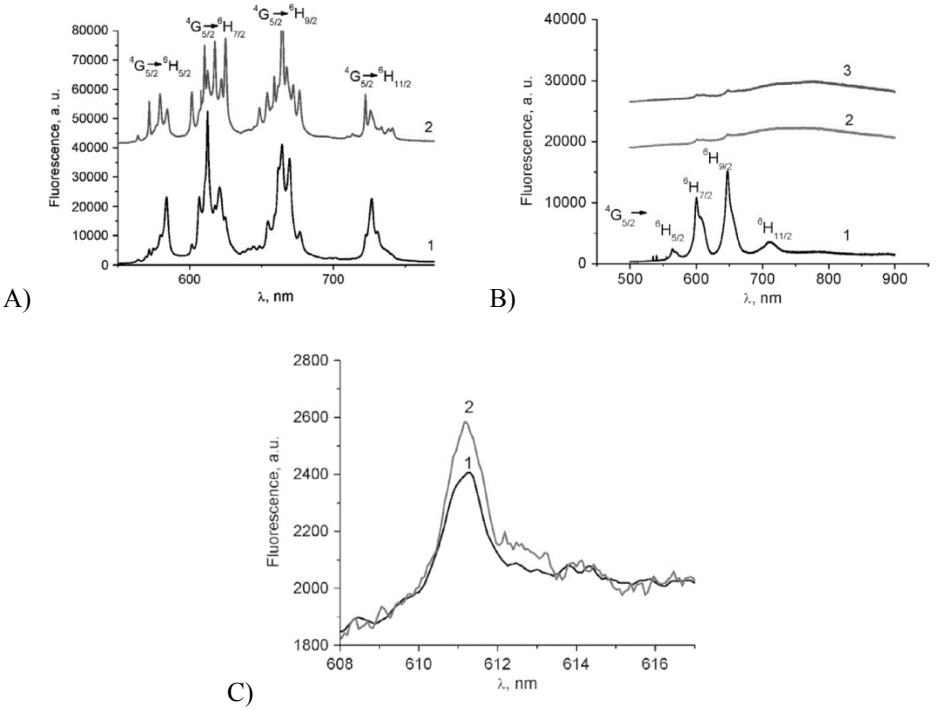

Figure 7. Photoluminescence spectra of TiO_2:Sm^{3+} and TiO_2:Sm^{3+} –Ag composite samples. A) λ_{ex} = 355 nm indirect excitation without plasmonic enhancement, B) λ_{ex} = 488 nm direct excitation without plasmonic enhancement and C) λ_{ex} = 410 nm excitation at plasmonic resonance of the substrate, with minor plasmonic enhancement of the signal. [49]

To understand the differences between the spectra of the direct and indirect excitations, micro-Raman scattering measurements were carried out. Raman scattering data gives information, which helps to determine the local crystalline structure of the prepared samples. The spincoated samples with doped and co-doped TiO_2 films are amorphous at first and the crystal structure is formed after

the gelation, drying and annealing cycle. The Raman data with the information on the crystal structure of the sample is depicted in Figure 8.

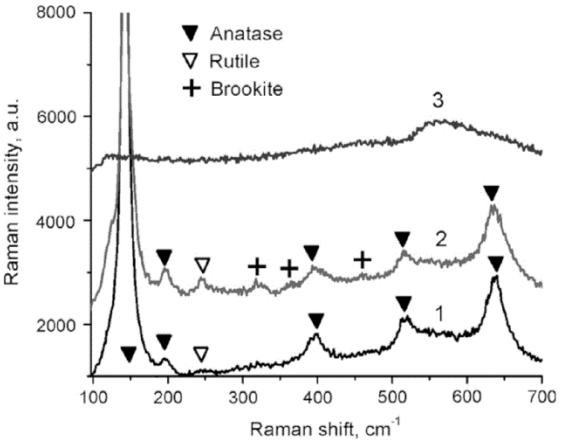

Figure 8. Micro-Raman measurement data of the doped and co-doped TiO_2 films. 1) TiO_2:Sm^{3+} film with Raman bands at 143, 196, 398, 518 and 639 cm^{-1}, which are typical for TiO_2 anatase crystalline structure. 2) TiO_2:Sm^{3+} –Ag film with modified Raman bands, with bands associated with rutile at 245 and 445 cm^{-1} and brookite at 323, 366 cm^{-1} crystal structure. The spectrum was measured at a silver aggregate. 3) TiO_2:Sm^{3+} –Ag film sample measured away from the silver aggregate. [49]

In the Figure 8 the spectrum 1 shows the TiO_2:Sm^{3+} films Raman signature and it is commonly associated with the anatase crystal structure of the TiO_2 host [83]–[85]. Spectrum 2, which depicts the micro-Raman data for TiO_2:Sm^{3+} –Ag film, measured near a silver aggregate differs from the previous spectrum. It has extra Raman bands associated with the rutile [83] and brookite crystal structure [86], [87]. Also some broadening of certain Raman bands is observed, which can be a manifestation of non-complete crystallisation of the co-doped samples. This is further exemplified by the spectrum 3, which was measured far away from silver aggregates and does not show any Raman bands associated with crystalline TiO_2 structure. The idea, that silver aggregates help the crystallisation of the TiO_2 host was confirmed by Raman mapping of the samples [49]. As the Raman measurements showed the presence of amorphous and crystalline features in the TiO_2:Sm^{3+} –Ag films it was expected, that also the fluorescence spectra are modified by the different phases.

The fluorescence spectrum measured with λ_{ex} = 355 nm from TiO_2:Sm^{3+} films depicted in Figure 7 shows narrow bands for split electron transitions: $^4G_{5/2} \rightarrow {}^6H_{5/2}$, $^4G_{5/2} \rightarrow {}^6H_{7/2}$, $^4G_{5/2} \rightarrow {}^6H_{9/2}$, $^4G_{5/2} \rightarrow {}^6H_{11/2}$ proving that the radiative Sm^{3+} ions are located in the TiO_2 anatase environment and these measurements are in accordance with the Raman scattering experiments [52], [83].

The fluorescence with λ_{ex} = 355 nm from co-doped TiO_2:Sm^{3+} –Ag films showed a modified spectrum, with extra narrow lines if compared to TiO_2:Sm^{3+} sample without the silver particles. It has been proposed, that these extra lines account for Sm^{3+} ions situated in a modified site in the anatase phase and these sites differ by the coordination of nearby oxygen vacancies [83]. The possibility of the formation of new complex optical centres must be also considered, which have been reported by Malashkevich et al. in a very similar structure [88]. The very sharp nature of these extra spectral lines suggests that the local environment of the emitting centres is still highly crystalline.

Under the direct excitation with 488 nm the fluorescence of the TiO_2:Sm^{3+} – Ag samples does not show the fine structure as with the indirect excitation. Only broad spectral features can be observed if measured at some silver aggregates and minor spectral peaks are seen in areas away from the silver aggregates. The broad nature of the spectral lines is common for the emitting centres, which are situated in disordered surroundings like amorphous and glassy host matrixes [89]. The direct excitation is considered to excite all the Sm^{3+} ions in the co-doped sample and the dominantly broad nature of the spectral bands proves that most of the ions are located in a disordered local environment. The statement is backed by the Raman scattering measurements, which showed the presence of crystalline phase only near the silver aggregates as depicted in Figure 8. A microscopic florescence mapping of the intensive $Sm3^{+}$ ion bands (at 600 and 647 nm) under direct excitation (λ_{ex} = 488 nm) showed that the local fluorescence signal was 20 times higher at silver aggregates than in sites away from the particles [49]. The enhancement is considered to be a complex phenomenon and it is more probable that it is caused by simple and complex silver ion centres, which transfer their energy non-radiatively to the samarium ions. Fluorescence measurements with λ_{ex} = 410 nm, which is in resonance with the localized plasmons yielded only around a 1.5 higher intensity near the silver aggregates. The lack of spectral overlap of $Sm3^{+}$ ion band with the plasmonic scattering spectrum in the main reason we do not consider the SPCE type enhancement of the emission. The samarium ions do not excite radiative plasmon modes in a considerable amount and thus does not account for the enhanced emission.

5.2. Enhanced fluorescence in RE doped oxides by incorporated gold core-shell nanoparticles

The discussion of fluorescence intensity enhancement by plasmonic structures yielded the result, that nanoparticles with higher scattering cross-sections are more suitable than small sub 50 nm nanoparticles, which have a relatively higher absorption cross-section and higher losses. In this section we present and analyse the effects of relatively big silica-gold core-shell nanoparticles on the emission of TiO_2:Sm^{3+} thin films.

The fabrication of the core-shell nanoparticles was based on the Ströber method followed by the covering of the core particles by a continuous gold film. The resulting nanoparticles were characterized by scanning electron microscope (SEM) measurements and yielded a size of the silica core approximately 140 nm and a thickness of the gold shell ca 15–20 nm (Figure 9 A). Extinction measurement of the nanoparticles dispersed in water showed pronounced maxima at 525 and 675 nm and closely resembles the calculated spectrum using Mie theory (Figure 9 B). Dark field imaging confirmed the plasmonic nature of the nanoparticles incorporated to the TiO_2 host matrix. Florescence imaging confirmed the existence of strong Sm3+ emission near the plasmonic particles. The comparison of dark field images with fluorescence images demonstrated an excellent spatial correspondence between the location of the highly scattering and fluorescing spots (Figure 10). Similar fluorescence images taken on films without the core-shell particles did not show the presence of bright spots. The lack of such bright spots in undoped TiO_2:Sm^{3+} thin films stands as evidence that the gilded nanoparticles participate in an enhanced emission Sm^{3+} ions.

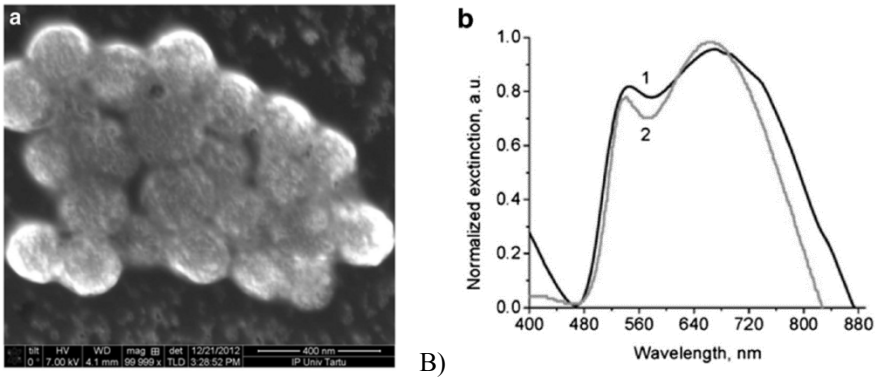

A) B)

Figure 9. A) SEM image of the fabricated core shell nanoparticles. B) Experimental (1) and theoretical (2) extinction spectra of the nanoparticles dispersed in water. [47]

The direct excitation measurements of local fluorescence with λ_{ex} = 355 nm near and away from these bright spots have the traditional shape of Sm^{3+} ions incorporated in TiO_2 with anatase structure. The results of the spectral acquisitions are depicted in Figure 11 and show approximately 10 times enhanced samarium spectra signal at the particles compared to the samarium ion situated in the area without plasmonic nanoparticles. Similarly to the case of silver nanoparticles covered in the previous section we cannot attribute the stronger signal to the simple plasmonic enhancement of electric fields as the excitation wavelength with 355 nm is of the resonance of the particles.

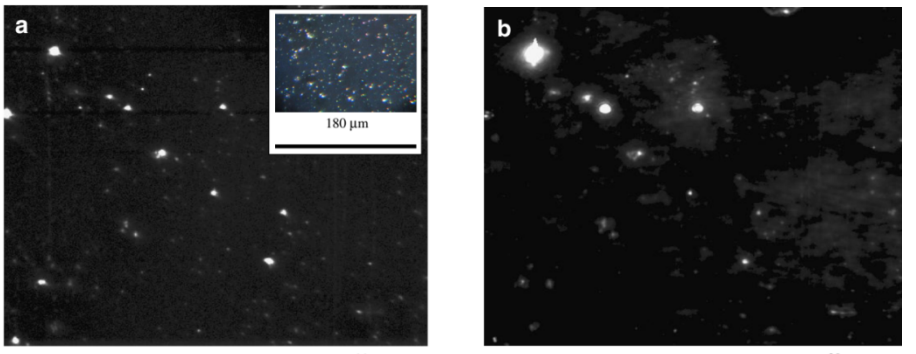

A) B)

Figure 10. A) Greyscale dark field scattering image. B) Greyscale fluorescence image from the same area as A) from TiO_2:Sm^{3+}-Au thin films with excitation wavelength λ_{ex} = 355 nm. [47]

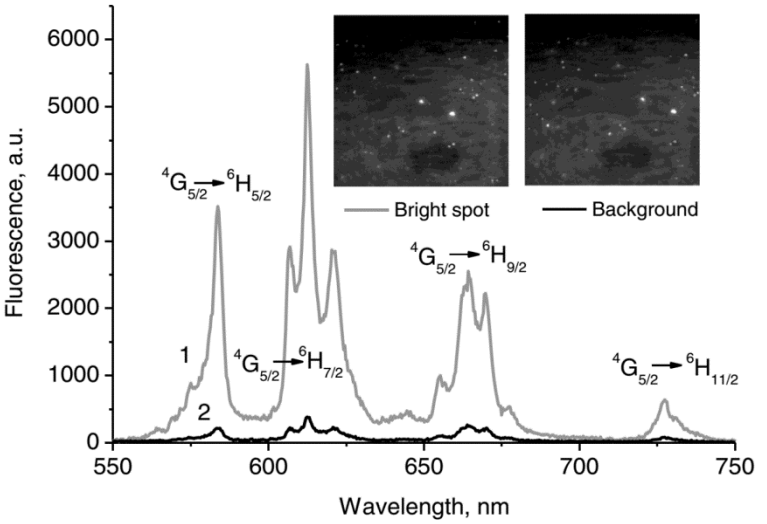

Figure 11. Micro-luminescence spectra of TiO_2:Sm^{3+}–Au films measured on a bright scattering particle (blue curve) and away from it from the background (black curve) with λ_{ex} = 355 nm. The insets show wide field fluorescence images from the measured areas. The exact measured points are in the centre of the images. [47]

The possible mechanism of metal mediated emission could be involved, but multiple measurement of fluorescence lifetime proved to be inconclusive. Although some lifetime measurements showed a certain degree of lifetime shortening there was a lack of a systematic trend and some locally measured lifetimes at the nanoparticles showed even an increased averaged lifetime. It was necessary to use three exponential decay components to satisfactorily

describe the measured decay kinetics. A sample decay curve is depicted in Figure 12 and some extra measurement results in the following Table 2. The fluorescence lifetime components with their values in the order of few hundred microseconds represented with τ_3 are typical for RE ions situated in a good quality anatase crystalline environment. The lifetimes in the order of tens of microseconds can correspond to samarium ions situated in the host having different crystallinity or are near local lattice defects. The average lifetimes for the measurements on the particle and off the particle did not differ considerably. Thus it is concluded that the radiative decay rate is not considerably changed by the plasmonic nanoparticles. The detected enhancement with the ultraviolet excitation could have different origins and the possibility of plasmon assisted non radiative energy transport to the samarium ions has to be considered. Recent publications have demonstrated non-radiative plasmon interactions involving enhancement of excitonic processes in improved photocatalysis. And also plasmon assisted Förster resonance energy transfer in quantum dot systems has been described.

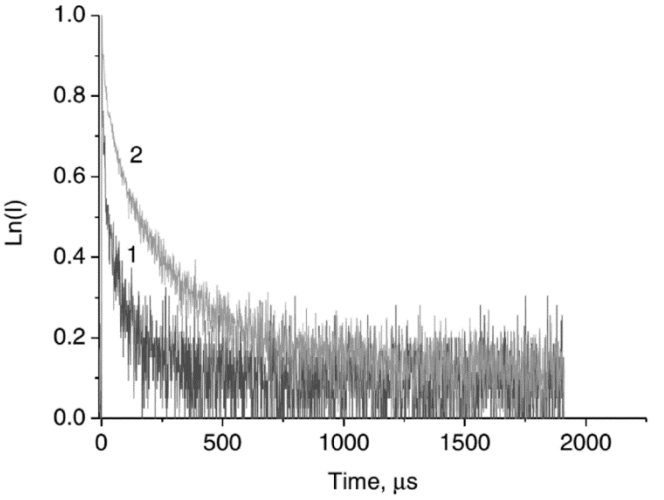

Figure 12. Normalized experimental fluorescence decay kinetics: from background (1), from bright spot (2) of TiO_2. [47]

Table 2. Lifetime components and averaged lifetime of fluorescence kinetics measurements of TiO_2:Sm^{3+}–Au thin films. [47]

Sample type	**τ_1, μs**	**τ_2, μs**	**τ_3, μs**	**τ, μs**
Particle 1	2.5	25	156	103
Particle 2	6.5	48	299	147
Particle 3	10.5	78	294	202
Background 1	4.1	35.3	225	138
Background 2	7.4	50	220	137

Direct excitation of the fluorescence with λ_{ex} = 355 nm yields a similar spectrum and is depicted in Figure 13. The spectra in this case consist of broader and almost featureless Sm^{3+} emission bands and are typical for the situation

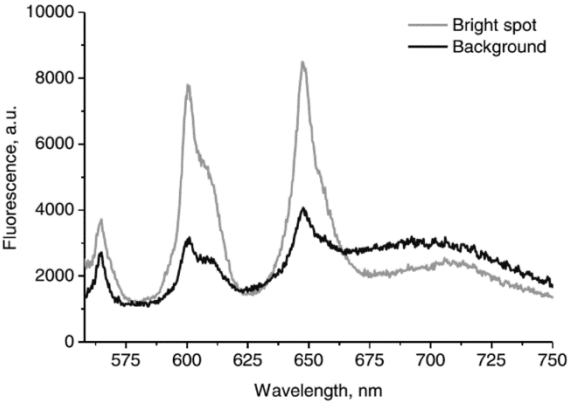

Figure 13. Micro-luminescence spectra of TiO_2:Sm^{3+}–Au films measured on a bright scattering particle (red curve) and away from it from the background (blue curve) with λ_{ex} = 532 nm. [47]

5.3. SPCE of photostable rare-earth doped metal oxide thin films

For the study of the SPCE phenomenon commercially available gold film substrates were covered with samarium doped TiO_2 thin films with various thicknesses (47, 64 and 100 nm). The 50 nm thick gold film covered glass substrates were bought from PHASIS (Switzerland). The sol-gel method was used in combination with spin coating to cover the gold side of the substrates with the TiO2:Sm3+ films. The thicknesses were estimated using transmittance spectra of reference samples without the gold layer [90]. These films were then attached to a semicylindrical BK7 prism, which was attached to a goniometric measurement system allowing the study of angular dependent fluorescence. For the SPCE experiments mostly the reverse Kreschman scheme was employed depicted in Figure 4 B. The samples were excited by the third harmonic of a Nd:YAG laser with λ_{ex} = 355 nm. A fibre coupled CCD spectrometer (Ocean Optics 2000) was connected to goniometric system. Angular and polarization dependent fluorescence spectra were recorded at the prism side of the setup in the range of 0°–90°. The degree of polarization was determined by using an analyser placed before the spectrometer. The degree of polarization was estimated by the ratio of minimal and maximal intensities given by

$$P = \frac{I_{max} - I_{min}}{I_{max} + I_{min}} \quad , \qquad (9)$$

where P denotes the degree of polarization an I_{max} and I_{min} are the maximal and minimal fluorescence intensities respectively registered by the spectrometer.

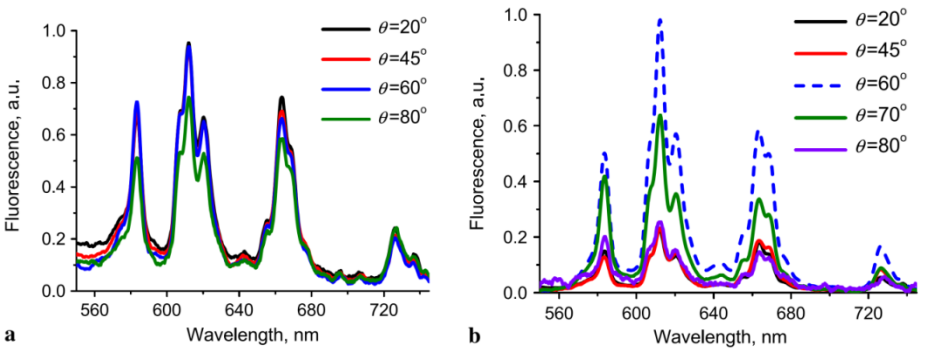

Figure 14. Normalized variable angle fluorescence spectra of TiO_2:Sm^{3+} thin films samples. a) TiO_2:Sm^{3+} thin film sample on pure glass attached to the semicylindrical prism; b) TiO_2:Sm^{3+} thin film sample on the gold-covered glass slides attached to the semicylindrical prism. [48]

Figure 14 depicts the dependence of the recorded fluorescence spectra on the detection angle of the spectrometer on two different samples. First a reference sample of a samarium doped TiO_2 thin film on a glass substrate attached to the prism setup was measured, which showed no significant dependence on the detection angle (Figure 14 A). In contrast the TiO_2:Sm^{3+} film on the gold covered glass slide showed a strong angle dependence of the signal (Figure 14 B). The fluorescence spectra showed the typical features for the TiO_2:Sm^{3+} system with pronounced peaks specific to Sm^{3+} ions with maximal intensities at 583, 616, 665 and 728 nm corresponding to the 4f–4f transitions. A very strong angle dependence of the gold film sample becomes evident in the $45° < \theta < 80°$ angular range. More exact measurements showed that the intensities of the different peaks of the Sm^{3+} ions depend non-monotonically on the detection angle. Each peak has a maximal value at a different angle. Thus, the metal-dielectric film system allows tailoring of the fluorescence spectrum by modifying the interrelation of the intensities of different fluorescence bands at different detection angles.

The more exact polarization and detection angle dependent measurements of the fluorescence intensities of the distinct pronounced emission wavelengths revealed two different types of radiation. The measurements revealed a strong dependence of the polarization and angular distribution properties of the radiation, which is sensitive to the film thickness of the TiO_2:Sm^{3+} layer spin

coated on top of the gold substrate. To understand the physical processes involved we used theoretical reflectance calculations of the layered and prism coupled system. The results of the measurements and calculations are depicted in Figure 15.

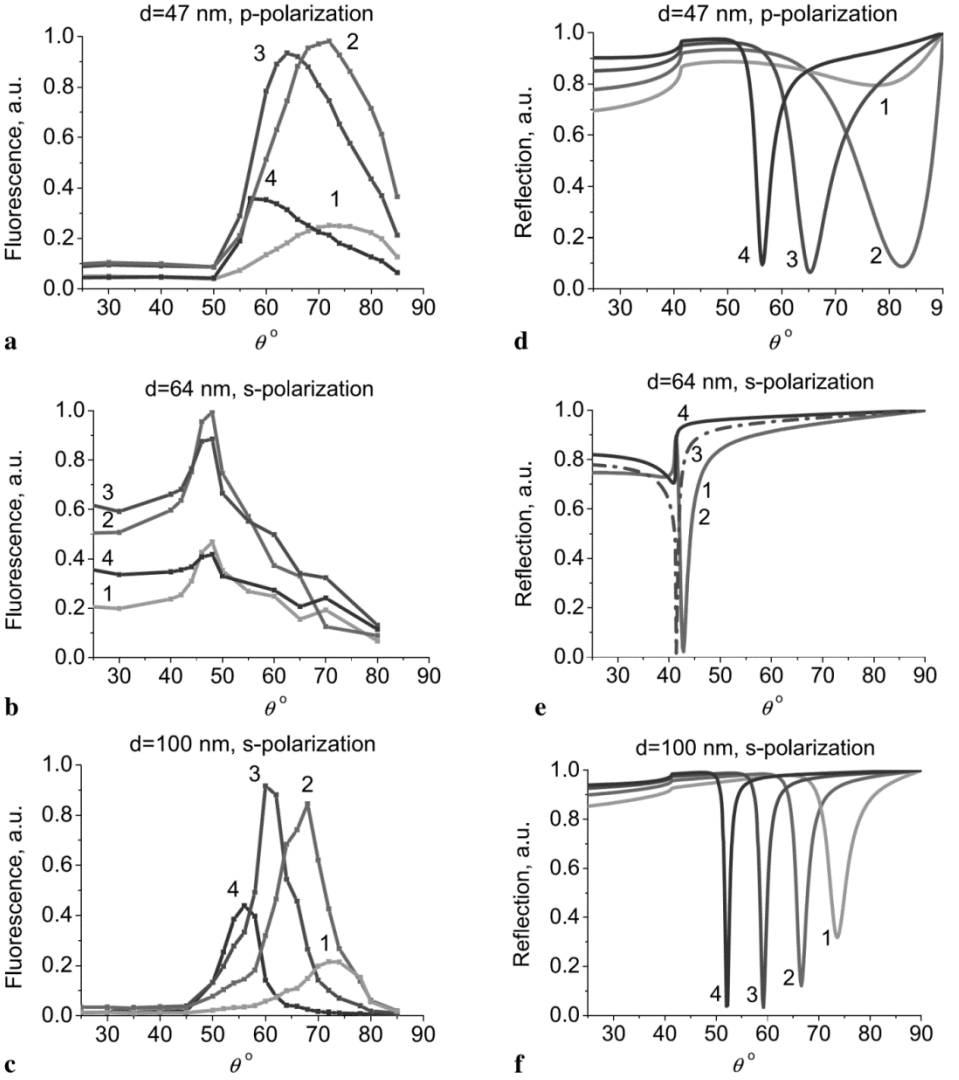

Figure 15. Measured angular dependence of the fluorescence (a–c) and calculated reflectance (d–f) of the metal-dielectric system of TiO_2:Sm^{3+} /50 nm Au/glass with varying thicknesses of the TiO_2:Sm^{3+} layer. Data for different spectral peaks are plotted: (1) 583 nm; (2) 616 nm; (3) 665 nm and (4) 728 nm. Also depicted in the plots are the polarization of the emission and the thickness of the TiO_2:Sm^{3+} film. [48]

The nature of the SPCE light as described in paragraph 2.2.2. is that the emitted radiation is p-polarized. P-polarized light was also registered in the experiment, but only in the case of the thinnest 47 nm thick TiO_2:Sm^{3+} layer sample. The thicker samples showed predominantly s-polarization emission. This corresponds to the coupling of the fluorescence to leaky waveguide modes inside the TiO_2 layer. The phenomenon can be understood with the help of the theoretical reflectance calculations of such a layered system. These show that the attenuated total reflection dips in the p-polarized reflectivity plots, which are attributed to the plasmonic modes on the gold-TiO_2 interface exist only for the thin 47 nm sample. The high effective dielectric constant of TiO_2 does not allow the necessary wavevector matching condition for the exciting of surface plasmon polaritons to be fulfilled for the thicker samples. The effective dielectric constant "felt" by the evanescent electric fields of the electromagnetic waves is low enough only in the thinnest sample. If the dielectric constant of the fluorescent layer would be lower than the glass/oil/prism substrate, then it is possible for both the surface plasmons and wave guide modes to be simultaneously excited. This has been previously showed in experiments with thick dielectric loaded plasmonic waveguides.

The data plotted in Figure 15 shows a good correlation between the angular positions of the minima in the calculated reflectivity curves at the specific wavelengths with the corresponding angular positions of the measured fluorescence intensity maxima at the same wavelengths. The minima of the reflectivity curves at these certain wavelengths correspond to the excitation of either leaky surface plasmon modes or the leaky wave guide modes. The same modes are excited by the fluorescence of the incorporated samarium ions and as the modes are leaky, they can out-couple at the certain angles, which are visible in the reflectivity calculation data. The degree of polarization for the coupled emission was in the range of 0.8–0.9. The metal dielectric structure studied, enables the redistribution of traditionally isotropic emission of the randomly oriented Sm^{3+} ions in a controlled manner. It is shown, that one can modify the polarization and angular distribution of the fluorescence by controlling the TiO_2:Sm^{3+} layer thickness of the sample. Although in the presented study of this geometric setup the fluorescence lifetimes of the different type of leakage radiation could not be investigated, it is believed that the also the lifetimes for the surface plasmon coupled and waveguide mode coupled radiation are modified and differ from the bulk TiO_2:Sm^{3+} sample. Combining the photostability of the fluorescence of Sm^{3+} ions in the TiO_2 host matrix and the possibility of controlled modification of the polarization, the angular distribution and possibly the fluorescence lifetimes it is proposed that rare earth doped oxides are of high importance for fundamental and experimental investigation of advanced leaky waveguide structures. A polarization and spectrally sensitive leakage radiation microscope combined with fluorescence lifetime imaging would be an ideal tool for such further experimentation.

5.4. Spectral reshaping of NV centre luminescence

One of the most intriguing phenomena of plasmon coupled emission is the spectral reshaping of fluorescence of the plasmon-coupled emitters [91]–[95]. This effect is based on the modification of the fluorescence spectra of the emitters, when placed near a plasmonic system, which has resonances overlapping some parts of the emission spectra of the emitter. The effect can be understood if considering equation (8) in paragraph 2.2.1. It is shown, that the enhancement of fluorescence intensity near a plasmonic particle depends on the scattering cross-section of the particle. The scattering cross-section is a wavelength dependent and thus the enhancement factor is also a wavelength dependent process. As differently shaped plasmonic nanoparticles of different materials can have diverse scattering cross-sections with very different wavelength dependent enhancement profiles, it is possible to selectively enhance some parts of the fluorescence spectra of the emitters. It is important to note, that the overall fluorescence spectra of the emitters coupled to a plasmonic system contain at least two different kind of radiation. The spectra are a mix of the intrinsic fluorescence profile with unpolarised light and of the plasmon-coupled emission, which is polarized in a way, which is determined by the radiative plasmons and is a very similar effect to SPCE.

This paragraph of the thesis was motivated by the reported lack of data on the spectral reshaping of fluorescence of plasmon-coupled emitters described by [25], and includes data, which has not yet been published. The studied system has been motivated by the recent publication by [81], where a commercially available SERS substrate was used for the modification of the fluorescence lifetime of emitters and to visualize the lifetime modification under a fluorescence lifetime imaging microscope.

5.4.1. Spectral reshaping of plasmon coupled single nanodiamonds

First the fluorescence spectra of single nanodiamonds with included fluorescent nitrogen vacancies are discussed. As described in paragraph 4.1.2., an ultra-sound pre-treated and diluted solution of FNDs in deionized water was drop coated on top of the Klarite SERS substrate and dried on a hotplate. The sufficient low concentration of the solution and quick drying resulted in adsorption of single nanodiamonds which were scattered around the substrate and covered the structured and smooth gold film regions of the Klarite substrate. The distance between single FNDs was enough to measure single particle spectra. Care had to be taken not to measure the small aggregates of single particles, which are coupled to one another and which are difficult to distinguish from single particles under a fluorescence microscope.

The excitation wavelength used in the fluorescence measurements and imaging was 523 nm from a second harmonic of a Nd:YAG solid state laser. The microscope used was a heavily modified microscope setup based on

Olympus BX41M microscope combined with an Andor iXon EMCCD camera for highly sensitive imaging and a fibre-coupled Andor SR303i spectrometer with Andor Newton camera for spectral measurements. The spatially filtered excitation beam allowed for wide field and focused excitation of FND fluorescence. The fibre-coupled spectrometer was aligned to measure the focus spot of the focused beam and the central position of the wide field illuminated region allowing the simultaneous measurement of fluorescence spectra of tightly localized area while imaging. The fluorescence was filtered with a 532 nm notch filter and a 550 nm long pass filter from Thor labs. For the exact positioning of the FNDs into the focus spot of the laser beam and the spectrometer a piezoelectric positioning system Nano–H100 from Mad City Labs Inc. was used allowing the positioning of the 140 nm FNDs in the focus with a used 5 nm precision. The measurement of fluorescence spectra was highly sensitive to the location of the nanodiamonds in respect to the focus spot and careful focusing procedure of every single nanodiamond was implemented to exclude chromatic aberration effects in spectral acquisitions.

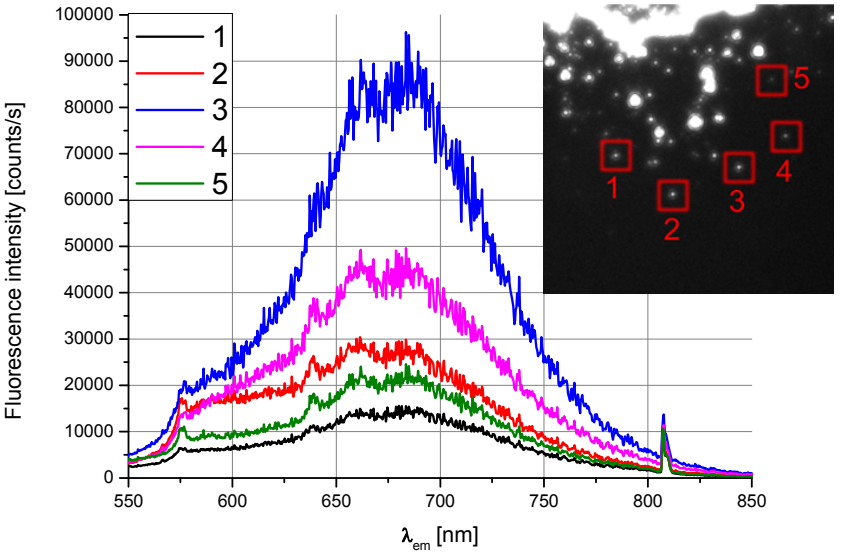

Figure 16. Fluorescence spectra of single nanoparticles deposited on the smooth Au regions of the Klarite SERS substrate. Although the intensities vary from particle to particle the spectral shape is almost the same for all particles. The small variations of the shape are mainly due to different fractional composition of NV^0 and NV^- centres in the particles. All spectra contain the distinctive ZPL features for the NV^0 and NV^- charge states. The sharp line at ca 810 nm is an unfiltered laser line. The inset shows the fluorescent image obtained using λ_{ex}=532 nm and shows the nanoparticles for the corresponding spectra.

To understand the plasmonic effects on the fluorescence of single FNDs baseline measurements were done for single nanodiamonds on the smooth gold film regions of the Klarite substrate. The inset of Figure 16 shows a drop coated area of the unstructured gold film, where FNDs can be observed as bright white spots. Single nanoparticle fluorescence spectra were measured away from aggregated nanodiamonds in the wide field illumination scheme. The corresponding spectra of the numbered nanodiamonds are depicted in Figure 16 and they differ mainly in their respective intensities. Small deviations in the shapes are explained by the different fractional composition of NV^0 and NV^- colour centres. These are very similar to typical room temperature fluorescence spectra of nanodiamonds containing NV colour centres, with the small peaks near 575 and 637 nm associated to the ZPLs of the NV^0 and NV^- optical complexes. Also typical for the FND is the shape of the phonon wing, this is in good agreement with previously published data. A sharp peak at ca 810 nm can be observed which is an unfiltered weak laser line.

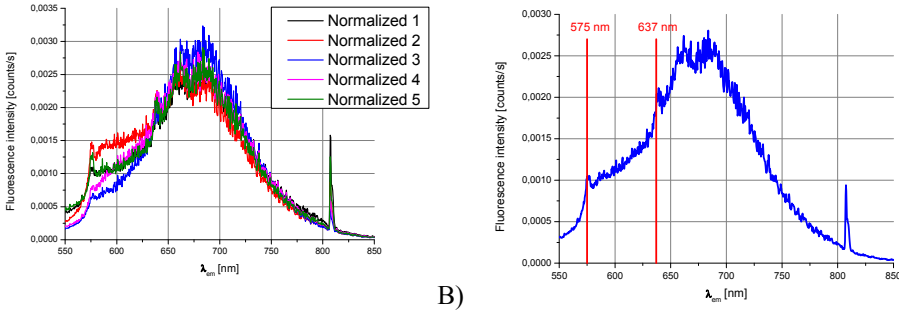

A) B)

Figure 17. A) Intensity normalized fluorescence spectra of single FNDs depicted in Figure 16 which gives a better view of the variations in the spectral shape in the 575–625 nm range. B) The intensity normalized and averaged spectrum of the 5 measured nanodiamonds on the smooth gold film with markers showing the ZPLs of the NV^0 and NV^- complexes at 575 and 637 nm respectively.

The intensity normalized fluorescence spectra of the corresponding single nanodiamonds are depicted in Figure 17 A, which gives an enhanced view of the small spectral shape differences of the measured particles. Figure 17 B shows the averaged spectrum of the five intensity normalized spectra. Also depicted are the positions of the zero phonon lines of the NV^0 and NV^- complexes at 575 and 637 nm. The noise in the measured fluorescence spectra is systematic and does not come from the lack of fluorescence signal. It disappears when measuring continuous samples and can be observed only in single particle measurements and shows interference type of behaviour. Figure 18 shows the comparison of the averaged and intensity normalized spectrum of the FNDs on the smooth gold film regions of the Klarite substrate to the spectrum of the FNDs placed on a normal microscope glass substrate.

There are only minor differences between these two spectra. The spectra of the highly reflective smooth gold film region contains an unfiltered laser line near 810 nm and has a higher background signal in the 550–650 nm region. Otherwise the spectra have an almost identical shape and display the typical ZPLs.

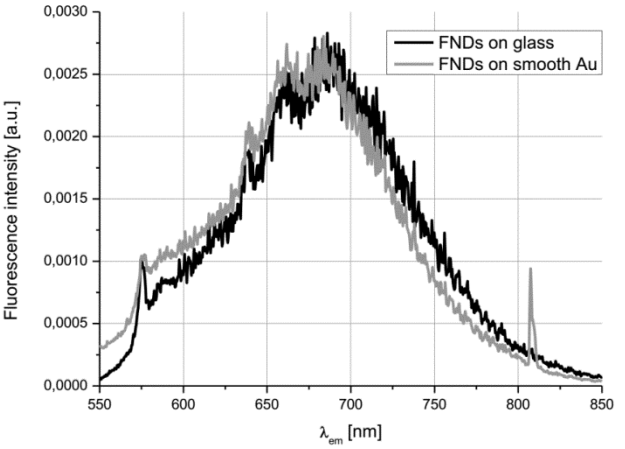

Figure 18. The comparison of the averaged and intensity normalized spectra of fluorescent nanodiamonds placed on top of a glass slide and the unstructured gold film on the Klarite substrate.

Figure 19 A and B show the drop coated single FNDs in the centre of wide field illumination scheme image (the central bright spots). They show FNDs on the structured gold film regions of the Klarite substrate. The spectral measurements were taken at the central position of the images and the data is presented in C. Two different measurements of the same nanoparticles are shown. The first spectral acquisition for each nanodiamond was done after a careful positioning of the nanodiamonds into the measurement spot to yield the highest signal. The second spectrum for each nanodiamond was registered after moving the sample stage and the following exact repositioning and focusing procedure. These double measurements show that after an exact repositioning routine the spectra are the same and chromatic aberration effects can be avoided. The spectra 1a and 1b in Figure 19 C show the data for the FND depicted in the centre of Figure 19 A.

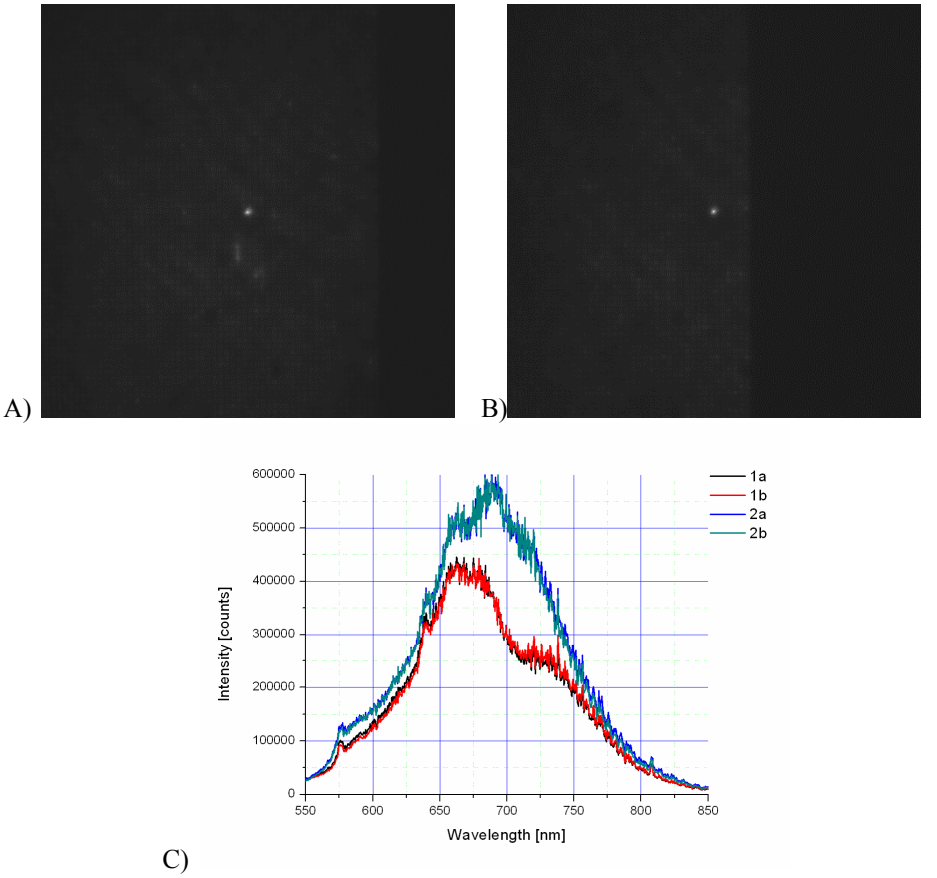

Figure 19. A) and B) depict fluorescence microscopy images of two different nanodiamonds deposited on the structured Klarite substrate area. C) depicts the recorded fluorescence spectra of the FND-s in the centre of images A) and B). Two spectra were measured for both particles to assure the correct positioning and focusing of the nanoparticles.

The recorded spectra form the nanodiamond depicted in Figure 19 A (spectra 1a and 1b) show a noticeably modified phonon wing. It exhibits an unusual feature for the nanodiamond spectrum near 700 nm and it is attributed to the metal induced spectral modification. The exact analysis of the positions of the FNDs yielded, that both of the drop coated nanodiamonds were not situated inside the pyramidal resonator. A previous study on molecules and small quantum dots had shown the drying process deposits the particles predominantly inside the pits and not on the area between them [96]. It is thought that in the case of the drop coating process the sticking of the FNDs in the areas between the pits is caused by the bigger size of the FNDs.

Experimental and theoretical studies combined with numerical simulations of such inverted pyramidal structures show a complex nature of the angular

dispersion of reflectance with a multitude of surface plasmon polariton and localized plasmon modes combined with diffractive features [97]–[99]. This complicates the analysis of the spectral modification shown in Figure 19 C. Especially as the nanodiamonds are not situated inside the resonant cavity and thus it is difficult to conclude, if this is a coupling phenomenon to surface plasmon or localized plasmon modes. To enhance the deposition of particles inside the pits spin coating with undiluted stock solution was used in the later stages of the experiments. The use of spin coating resulted in big areas of the structured part of the Klarite substrate where nanodiamonds were deposited inside the pits, but it is not guaranteed, that the pits are filled with just one nanodiamond. Figure 20 depicts the fluorescence spectra of single pits filled with nanodiamonds with the corresponding exact measured locations. One can see high variance of the shape of the measured spectra, which is believed to be caused by different local electromagnetic environment of the measured FNDs. This is a reasonable assumption as the FNDs are in different locations inside the micro voids and also the surface roughness is quite big as these structures are specialized for SERS measurements. The roughened surface has local hot spots with very different local plasmonic resonances.

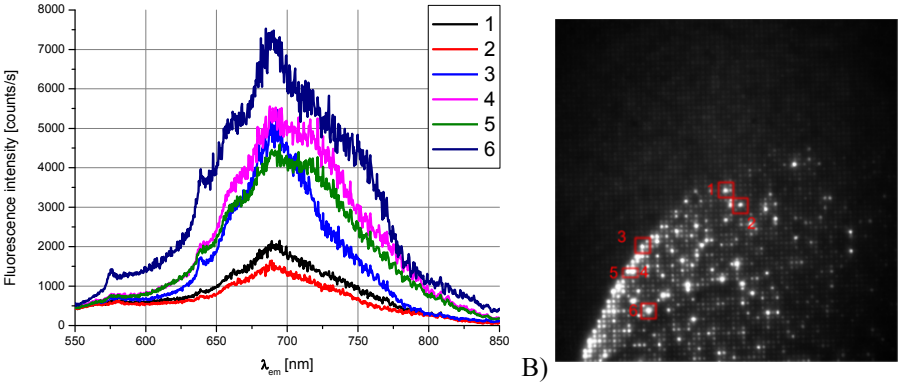

Figure 20. A) Locally measured fluorescence spectra of single pyramidal pits with FNDs inside. B) The measured locations corresponding to the measured spectra.

To get a better overview of the shape modification of the FND spectra we employed intensity normalization and averaging over the 6 measured spectra and compare the results with the normalized and averaged spectra of FNDs situated on the smooth gold film.

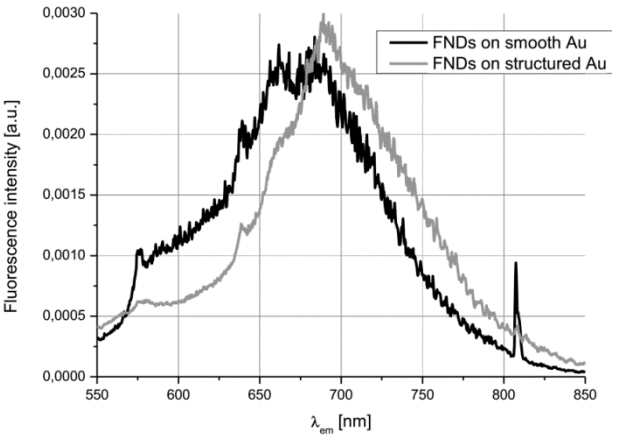

Figure 21. Comparison of the normalized and averaged fluorescence spectra of FNDs inside the pyramidal pits of the structured area (Red) and the FNDs on top of the smooth gold film area (Black) of the Klarite SERS substrate.

Figure 21 shows clearly a reshaping of the fluorescence spectra of nanodiamonds, which are situated inside the pyramidal pits which support localized plasmon modes. One can observe a noticeable change in the phonon wing structure with a distinct peak near 690 nm. The ZPLs for the NV^0 and NV^- are still visible and assuring that the measured spectra originates from these complexes. The most obvious changes are the relative increase of the intensity of the phonon wing peaking at around 690 nm. This is accompanied with the relative decrease of the intensities in the 575–675 nm range. The increase of the phonon wing intensity at 675–850 nm range is associated with relaxation processes involving plasmonic modes of the structure. To confirm this hypothesis one needs exact lifetime measurements. The lifetime measurements (not shown) using a frequency domain fluorescence lifetime imaging microscope on these covered substrates resulted in a very low signal. This was caused by the relative low efficiency of fluorescence of the NV complexes compared to regular fluorescence dyes. Thus the signal was too noisy for any conclusive validation of the hypothesis. Other possible factors that could account for the spectral reshaping phenomena are the spectrally dependent diffusive and normal incidence reflectivity of the structured samples, which could also produce modifications in the spectra [97]–[99]. As described the fibre coupled system was highly sensitive to precise focusing and positioning of the emitters into the focusing point. Although careful focusing and positioning procedure was followed there exists a minute possibility that the altered signal originates from a spectrally dependent detection efficiency of emitters on such a corrugated substrate. Very similar spectra obtained with a different measurement setup (presented in 5.4.2.) are the basis that we neglected the latter effect with high certainty.

5.4.2. Spectral reshaping of plasmon coupled ensemble of nanodiamonds

The ensemble measurements of fluorescence originating from the nanodiamonds situated on the smooth and structured areas of the Klarite substrate showed very similar behaviour as the single particle and pit experiments. The measured areas are the same as depicted in Figure 16 and Figure 20. The spectral measurements were done with the InVia micro Raman measurement system from Renishaw. A defocused 488m nm laser beam was used to coarsely map the nanodiamond fluorescence spectra of the smooth and structured parts of the Klarite substrate. The excitation spot diameter was around 20 µm. Bright field images of the measured samples can be seen in Figure 22. The greyscale overlay depicts the overall fluorescence intensity map of the structured and smooth parts of the substrate covered with FNDs. Spectra with the highest signals were used in the comparison between the fluorescence of FNDs situated on the different regions of the substrate and are presented in Figure 23.

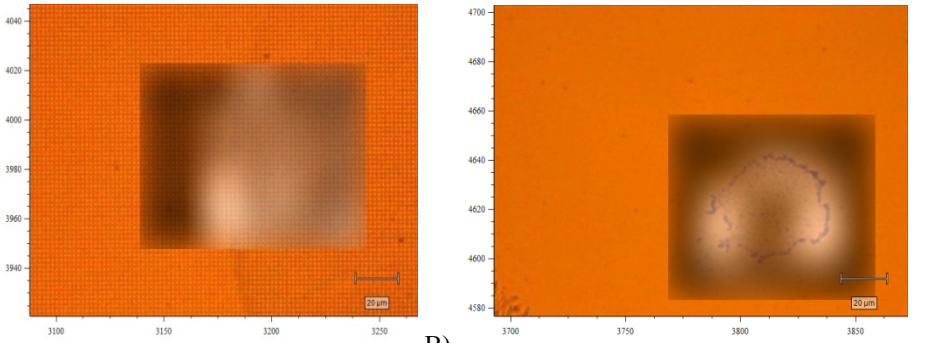

A) B)

Figure 22. A) A microscope image of a structured region of the Klarite substrate half of which is covered with NV centre containing FNDs and has a greyscale overlay map of the fluorescence intensity. B) A microscope image of a smooth region of the Klarite substrate which is covered with NV centre containing FNDs and has a greyscale overlay map of the fluorescence intensity. The scale bar in both images is 20 µm.

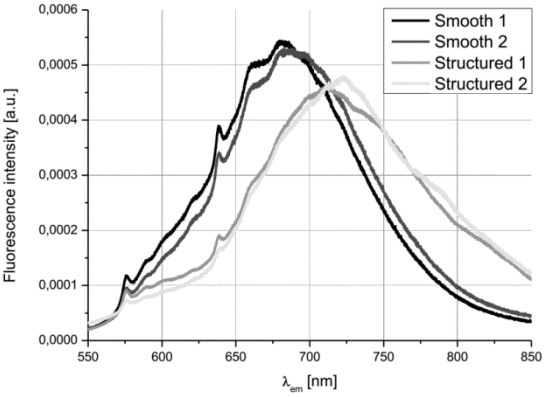

Figure 23. Modification of NV centre photo luminescence spectra of fluorescent nanodiamonds. The Smooth 1 and Smooth 2 spectra depict the two intensity normalized measurements of luminescence of nanodiamonds placed on the smooth Au film region on the Klarite substrate. The Structured 1 and Structured 2 intensity normalized spectra measured on the structured part of the substrate depict a modified shape. The easily noticeable spectral modifications overlap with the plasmon associated features in the reflectance measurements of the Klarite substrate shown in Figure 25.

The comparison of the FNDs spectra on the structures and the smooth part of the Klarite substrate yields clearly noticeable differences. The spectra of the FNDs situated on the structured surface show a shifted maxima and relative decrease of the short wavelength and relative increased signal of the long wavelength region. The modifications are similar to spectra of single nanodiamonds or voids which also possess a red shifted maximum and decreased short wavelength intensity. The red shifted maximum of the ensemble measurements is broader and the peaks near 700–725 nm and shape varies slightly by measurement to measurement. The averaged signal over all the mapping points for FNDs on structured and unstructured gold without the normalization procedure is shown in Figure 24. Although the recorded intensity of FND fluorescence on the structure was higher one cannot report an enhanced fluorescence signal with full confidence. This is due to the fact that the exact number of FNDs is unknown for both substrate types. That is why the intensity normalized spectra are preferentially analysed.

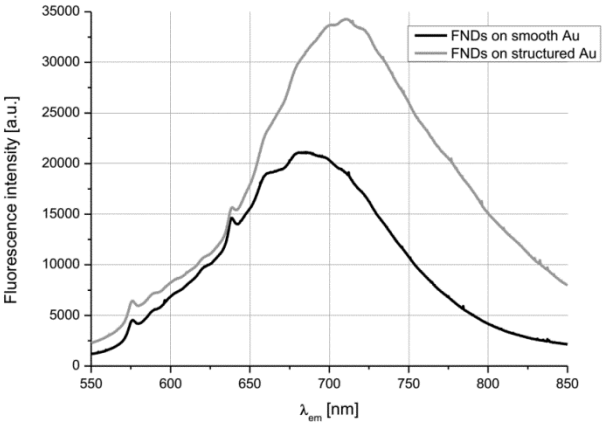

Figure 24. Averaged fluorescence intensities of the mapped regions depicted in Figure 22. The averaged signal is stronger on the structured surface and the maximum of the spectrum is shifted to longer wavelengths.

In order to better understand the processes involved in the spectral reshaping, we measured the normal incidence reflectivity of the Klarite substrate. The measured normal incidence reflectivity of a clean Klarite substrate has a noticeable wavelength dependent behaviour and is typical for such inverted pyramidal structure. The reflectivity data (shown in Figure 25) is very similar with previously reported experimental and theoretical studies [97]–[99]. It is interesting to note that there is a disagreement in the literature. Authors of [97], [99] argue, that the pit localized surface plasmons are associated with the dips in the specular reflection measurements and authors of [98] argue, that the peaks in the normal incidence reflectivity should be associated with the localized plasmon modes. The manufacturer of the SERS substrates recommends to use Raman excitation wavelengths 633 and 785 nm which fall to the shorter wavelength side of the reflection peaks, making the optimized enhanced Raman signal overlap with the maximum of the peaks. Therefore it is concluded that the peaks overlap with the radiative pit localized surface plasmon modes and effective surface plasmon coupled emission in the normal incidence regime is obtained at the maximal values on the peaks. From the fluorescence measurement data (Figure 25) an evident shift of the maximal position of the FNDs spectrum can be seen which is at first glance overlapping more with the minima than the maximal value in the reflectance measurement. But as the reflectance measurements were done on a clean substrate the red shift of the plasmon modes due the higher effective refraction index induced by the nanodiamonds inside the pits is not accounted for.

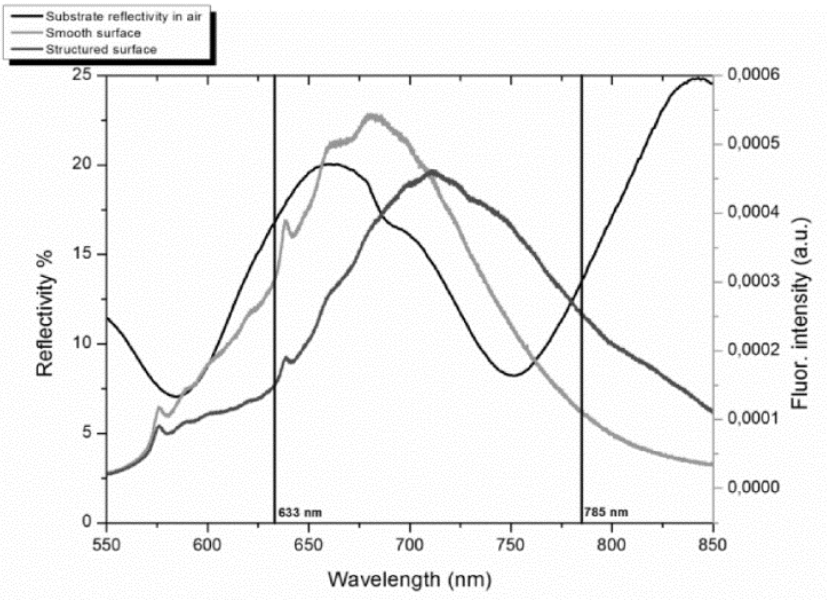

Figure 25. Normal incidence reflectivity spectrum (black) overlaid by the intensity normalized fluorescence spectra measurements of nanodiamonds on the structured part of the sample (dark grey) and on the smooth gold film area (light gray). Also depicted vertical lines are the manufacturers recommended wavelengths for SERS measurements showing that the optimum SERS enhancement region is situated on the peaks of the reflectivity curve.

Based on the numerical simulation data and theoretical analysis of [98] it is proposed, that the modified spectra of the FNDs on the structured part of the Klarite substrate are caused by pit localized radiative higher order plasmon modes which effectively enhance the phonon wing region of NV complex fluorescence. It is sad that further proof of this could not be given by fluorescence lifetime imaging measurements, as our equipment was not sensitive enough to give reliable lifetime measurement data.

6. CONCLUSION

We report the successful fabrication of photostable fluorescent TiO_2:Sm^{3+} thin films with high refractive index using the sol-gel fabrication method. This wet chemistry method enables the co-doping of the fluorescent matrix with metallic nanoparticles and when combined with the spin coating procedure it can be applied in the fabrication of layered structures suitable for studying waveguiding and surface plasmon-coupled emission phenomena.

Locally enhanced fluorescence intensities were registered for the fluorescent TiO_2:Sm^{3+} thin film samples with incorporated plasmonic metal nanoparticles. Fluorescence measurements with the direct and indirect excitation schemes of the Sm^{3+} ions revealed a maximum local enhancement of the fluorescence intensity by 20 times. The maximal signal enhancement Sm^{3+} ions was obtained with TiO_2:Sm^{3+} thin films co-doped with silver nanoparticles and with the direct excitation scheme with λ_{ex} = 488 nm. Co-doping the samples with silver nanoparticles induces the formation of micro-aggregates which disturb the homogenous anatase crystalline structure of the fluorescent TiO_2:Sm^{3+} thin films. Raman scattering measurements showed the mainly amorphous nature of the TiO_2:Sm^{3+}–Ag samples with a mix of anatase, rutile and brookite phases in the vicinity of silver aggregates. The enhancement of Sm^{3+} emission with with λ_{ex} = 488 nm is more likely connected with the presence of silver ions than with plasmonic effects. The direct excitation resulted in broad and featureless fluorescence spectrum of Sm^{3+} ions which originates from samarium situated predominantly in an amorphous environment.

In contrast the indirect excitation of TiO_2:Sm^{3+} with λ_{ex} = 355 nm results in a spectrum with pronounced sharp features which is associated with samarium ions enclosed in a crystalline anatase lattice. The measurements with λ_{ex} = 355 nm in the vicinity of silver aggregates show a modified spectrum with extra narrow lines and results also in an enhanced fluorescence of Sm^{3+} ions. The extra lines originate from different emission centres which probably differ by the coordination of charge-compensating oxygen vacancies and causes splitting of f–f transitions. Excitation with λ_{ex} = 410 nm overlapping the plasmonic resonance band of the silver nanoparticles yielded in a fluorescence enhancement of 1.5 times and provides the evidence that plasmon enhanced absorption is overshadowed by other sensitizing effects in these systems.

Measurements with TiO_2:Sm^{3+} films co-doped with successfully synthesised silica-gold core-shell nanoparticles yielded also locally enhancement of fluorescence of Sm^{3+} ions. Indirect excitation with λ_{ex} = 355 nm produced higher enhancement than with direct excitation with λ_{ex} = 532 nm. The local fluorescence intensity was approximately 10 times higher near the core-shell particles in the case of indirect excitation and about 2.5 times in the case of direct excitation. The achieved local enhancement in Sm^{3+} fluorescence can be explained by two plasmonic effects. First is plasmonically increased direct absorption of 532 nm light by Sm^{3+} ions. The second is the plasmonically

enhanced energy transfer from the excitons in TiO_2 host induced by UV light (355 nm) to the Sm3+ ions. The fabricated fluorescent TiO_2:Sm^{3+} thin film layered waveguide and plasmonic waveguide structures showed controllable emission from RE ions. We successfully demonstrated the coupling of narrow band Sm^{3+} ion emission to leaky surface plasmon and waveguide modes. It is possible to tune the polarization and angular properties of the emission by changing the thickness of the TiO_2:Sm^{3+} thin film. It is demonstrated in this thesis that placing fluorescent nanodiamonds containing nitrogen vacancy colour centres on nanostructured plasmonic substrates can cause considerable modifications to the fluorescence spectrum. Single nanoparticle and ensemble measurements show that the spectral modifications originate from the interaction with the structured gold surface. It is proposed that the near-field coupling of the NV centre fluorescence to radiative localized surface plasmon modes is the main contributor to the recorded spectral reshaping.

SUMMARY

The present thesis includes an experimental study of the modification of the emission of photostable emitters induced by nanometallic structures supporting plasmon modes. The theoretical part of this work describes the plasmonic effects on fluorescence and analyses the behaviour of plasmon-fluorophore coupled systems. The systems studied in this thesis are comprised of plasmonic structures coupled with the fluorescence of photostable or non-bleaching emitters. Most of the articles in the field of plasmonics, which deal with the interaction between plasmons and fluorescence emission study predominantly systems with traditional organic dye molecules in low refractive index materials. These dye molecules are usually not photostable and can suffer from photo bleaching, which restricts their range of application in plasmonic systems. The thesis at hand considers photostable fluorescent materials, which have a high refractive index and are less studied in the plasmonics literature. The fluorescence of titatnium oxide films doped with fluorescent samarium 3+ ions with incorporated plasmonic silver nanoparticles, gold core-shell nanoparticles and films covered on top of a thin gold layer are characterized. Also included in the thesis is the a study of a system comprised of fluorescent nanodiamonds containing NV-centres, which were placed on a nano- and micro structured gold substrate possessing plasmonic modes resonantly overlapping with the NV-centres fluorescence.The main focus was to investigate the possible effects of plasmonic structures on the emission characteristics of the fluorescent materials like the fluorescence intensity, the spectral shape, the angular distribution of the emission and modification of fluorescence lifetimes. It was found that TiO_2:Sm^{3+} films co-doped with silver and gold nanoparticles produce locally enhanced emission, but the plasmonic effects alone do not explain the entire observed enhancement. Direct excitation of Sm^{3+} ions in silver doped samples with λ_{ex} = 488 nm yielded a locally increased fluorescence intensity of up to 20 times. The enhancement cannot be explained by purely plasmonic enhancement of absorption or by the SPCE phenomenon and originates with high probability from traditional non-radiative energy transfer between silver and samarium ions and photoactive complexes comprised of these ions. In the the gold doped samples and in the indirect excitation of silver samples part of the enhancement is caused by plasmonic increase in Sm3+ direct light absorption in the vicinity of noble metal dopants or better energy transfer from light induced excitons in TiO2 host to Sm^{3+} ions. It was found that by changing the thickness of TiO_2:Sm^{3+} films situated on top of a 50 nm thick gold layer, it is possible to control if the narrowband emission of Sm^{3+} ions couples to surface plasmon or waveguide modes. The reversed Kretschmann scheme was employed for the characterization of the different type of polarization for fluorescence-coupled leaky SPCE and waveguide modes. The tuning of the fluorescent layer thickness results in controllable modification of the polarization and angular distribution of the emission. Spectral reshaping of photostable fluorescent

nanodiamonds is also demonstrated, which is induced by localized surface plasmon modes located on inside the pyramidal pits of the nanostructured Klarite substrates. Single particle and pit fluorescence imaging and spectral measurements combined with ensemble measurements show noticeable modified fluorescence spectra.

SUMMARY IN ESTONIAN

Nanometalliliste struktuuride poolt põhjustatud muutused fotostabiilsete fluorofooride kiirguses ja spektri kujus

See väitekiri käsitleb metall-dielektrik-pindadel levivate ja lokaliseeritud pinnaplasmonite vastasmõju fotostabiilsete kiirguritega. Töö teoreetilise ülevaate osas kirjeldatakse plasmonite mõju fluorestsentskiirgusele ning analüüsitakse plasmon-fluorofoor sidestatud süsteemi käitumist. Uurimise all olid plasmoonsed süsteemid, kus pinnaplasmonid või lokaliseeritud pinnaplasmonid on sidestatud fotostabiilsete ehk mittepleekivate kiirgustsentrite fluorestsentsiga. Senised plasmoonika valdkonna uurimused, mis käsitlevad plasmonite ja fluorestsentskiirguse vastasmõju, on põhinenud enamjaolt vaid tavapärastel orgaanilistel värvainemolekulidel, mis paiknevad madala murdumisnäitajaga keskkondades. Need molekulid ei ole üldiselt fotostabiilsed ja pleegivad kiiresti ning see piirab nende rakendamist plasmonitega sidestatud süsteemides. Käesolevas uurimustöös keskendutakse fotostabiilsetele kiirgavatele materjalidele, mis on suure murdumisnäitajaga ning mida on senises teaduskirjanduses vähem käsitletud. Väitekirjas iseloomustatakse sool-geel-meetodil valmistatud samaariumi 3+ (Sm^{3+}) ioonidega dopeeritud titaanoksiidist (Sm^{3+}:TiO_2) kilede fluorestsentsi, kui need fluorestseerivad kiled on vastasmõjus plasmoonsete hõbedast nanoosakestega, kullast kiledega ja kihiliste kullast nanoosakestega. Lisaks vaadeldakse ka süsteemi, mis koosneb lämastik-vakants- (NV) kiirgustsentreid sisaldavatest nanoteemantidest. Nanoteemandid on paigutatud nano- ja mikroskaalas struktureeritud kullast kiledele, millel eksisteerivad NV-tsentrite fluorestsentsiga kattuvad resonantsed pinnaplasmonite moodid.

Peamiselt vaadeldi plasmonstruktuuride mõju fluorestseerivate materjalide kiirguskarakteristikutele, nagu näiteks intensiivsus, fluorestsentsspektri kuju, kiirguse ruumiline jaotus ja kiirguse eluiga. Leiti, et hõbeda nanoosakestega dopeeritud Sm^{3+}:TiO_2 kilede puhul hõbeda nanoosakesed võimendavad kiirgust, kuid plasmonite põhjustatud võimendus ei selgita kogu intensiivsuse suurenemist. Sm^{3+} otsesel ergastamisel lainepikkusel 488 nm registreeriti fluorestsentskiirguse lokaalne intensiivsuse kuni 20-kordne suurenemine ning demonstreeriti, et see võimendus ei ole seletatav ainult plasmonite võimendatud neeldumise ega pinnaplasmonitega sidestatud kiirguse SPCE (Surface plasmon-coupled emission) kaudu. Seega on antud juhul intensiivsuse kasvu suure tõenäosusega põhjustanud traditsiooniliste mittekiirguslike energiaülekande protsessidega hõbeda ja samaariumi ioonid ning neist moodustunud fotoaktiivsed ühendid. Kullaga dopeeritud ja kaudse ergastusega hõbedaga proovide fluorestsents on osalt plasmonite poolt võimendatud. Seda tingib otsesel ergastusel neeldumise kasv kuldosakeste lähedal ja efektiivsem energiaülekanne eksitonidelt kaudsel ergastusel. Leiti, et 50 nm paksustele kullast kiledele kaetud Sm^{3+}:TiO_2 kihtide paksuse muutmisega on võimalik juhtida seda, kas Sm^{3+} ioonide peenestruktuurne kiirgus sidestub plasmonmoodidega või

lainejuhi moodidega. Pööratud Kretschmanni skeemi kasutava katseseadmega määrati, et SPCE tüüpi lekkekiirgus ja lainejuhi moodidega sidestatud kiirgus on erineva polarisatsiooniga. Fluorestseeriva kihi paksuse muutmisega saab juhtida lekkekiirguse polarisatsiooni ning nurksõltuvusi. Lisaks demonstreeriti fotostabiilsete nanoteemantite fluorestsentsspektri kuju muutusi, mis on põhjustatud struktureeritud Klarite substraadi püramiidsetes aukudes asuvate lokaliseeritud pinnaplasmonite moodide poolt. Üksikute osakeste ja üksikutes aukudes asuvate osakeste fluorestsents mõõtmised koos mõõtmistega suuremalt pinnalt demonstreerisid selget spektraalkuju muutst.

REFERENCES

[1] D. Sarid and W. Challener, *Modern Introduction to Surface Plasmons*. Cambridge: Cambridge University Press, 2010.

[2] S. A. Maier, *Plasmonics: Fundamentals and Applications*. Boston, MA: Springer US, 2007.

[3] G. Mie, "Beiträge zur Optik trüber Medien, speziell kolloidaler Metallösungen," *Ann. Phys.*, vol. 330, no. 3, pp. 377–445, 1908.

[4] R. Ritchie, "Plasma Losses by Fast Electrons in Thin Films," *Phys. Rev.*, vol. 106, no. 5, pp. 874–881, Jun. 1957.

[5] R. W. Wood, "On a Remarkable Case of Uneven Distribution of Light in a Diffraction Grating Spectrum," *Proc. Phys. Soc. London*, vol. 18, no. 1, pp. 269–275, Jun. 1902.

[6] Y. Wang, E. W. Plummer, and K. Kempa, "Foundations of Plasmonics," *Adv. Phys.*, vol. 60, no. 5, pp. 799–898, Oct. 2011.

[7] U. Kreibig and M. Vollmer, *Optical Properties of Metal Clusters*, vol. 25. Berlin, Heidelberg: Springer Berlin Heidelberg, 1995.

[8] K. L. Kelly, E. Coronado, L. L. Zhao, and G. C. Schatz, "The Optical Properties of Metal Nanoparticles: The Influence of Size, Shape, and Dielectric Environment," *J. Phys. Chem. B*, vol. 107, no. 3, pp. 668–677, Jan. 2003.

[9] C. Noguez, I. O. Sosa, and R. G. Barrera, "Optical Properties of Metal Nanoparticles with Arbitrary Shapes," *J. Phys. Chem. B*, vol. 107, no. 26, pp. 6269–6275, Jul. 2003.

[10] P. L. Stiles, J. A. Dieringer, N. C. Shah, and R. P. Van Duyne, "Surface-enhanced Raman spectroscopy.," *Annu. Rev. Anal. Chem. (Palo Alto. Calif).*, vol. 1, pp. 601–26, Jan. 2008.

[11] S. Nie, "Probing Single Molecules and Single Nanoparticles by Surface-Enhanced Raman Scattering," *Science (80-.).*, vol. 275, no. 5303, pp. 1102–1106, Feb. 1997.

[12] K. Kneipp, H. Kneipp, I. Itzkan, R. R. Dasari, and M. S. Feld, "Surface-enhanced Raman scattering and biophysics," *J. Phys. Condens. Matter*, vol. 14, no. 18, pp. R597–R624, May 2002.

[13] M. Moskovits, "Surface-enhanced spectroscopy," *Rev. Mod. Phys.*, vol. 57, no. 3, pp. 783–826, Jul. 1985.

[14] M. Fleischmann, P. J. Hendra, and A. J. McQuillan, "Raman spectra of pyridine adsorbed at a silver electrode," *Chem. Phys. Lett.*, vol. 26, no. 2, pp. 163–166, May 1974.

[15] D. L. Jeanmaire and R. P. Van Duyne, "Surface raman spectroelectrochemistry," *J. Electroanal. Chem. Interfacial Electrochem.*, vol. 84, no. 1, pp. 1–20, Nov. 1977.

[16] B. Sharma, R. R. Frontiera, A.-I. Henry, E. Ringe, and R. P. Van Duyne, "SERS: Materials, applications, and the future," *Mater. Today*, vol. 15, no. 1–2, pp. 16–25, Jan. 2012.

[17] E. Fort and S. Grésillon, "Surface enhanced fluorescence," *J. Phys. D. Appl. Phys.*, vol. 41, no. 1, p. 013001, Jan. 2008.

[18] C. D. Geddes, I. Gryczynski, J. Malicka, Z. Gryczynski, and J. R. Lakowicz, "Directional Surface Plasmon Coupled Emission," *J. Fluoresc.*, vol. 14, no. 1, pp. 119–123, Jan. 2004.

[19] J. R. Lakowicz, “Radiative Decay Engineering: Biophysical and Biomedical Applications,” *Anal. Biochem.*, vol. 298, no. 1, pp. 1–24, Nov. 2001.
[20] J. R. Lakowicz, “Radiative decay engineering 5: metal-enhanced fluorescence and plasmon emission,” *Anal. Biochem.*, vol. 337, no. 2, pp. 171–194, Feb. 2005.
[21] I. Gryczynski, J. Malicka, Z. Gryczynski, and J. R. Lakowicz, “Radiative decay engineering 4. Experimental studies of surface plasmon-coupled directional emission,” *Anal. Biochem.*, vol. 324, no. 2, pp. 170–182, Jan. 2004.
[22] J. R. Lakowicz, “Radiative decay engineering 3. Surface plasmon-coupled directional emission,” *Anal. Biochem.*, vol. 324, no. 2, pp. 153–169, Jan. 2004.
[23] J. R. Lakowicz, Y. Shen, S. D’Auria, J. Malicka, J. Fang, Z. Gryczynski, and I. Gryczynski, “Radiative Decay Engineering,” *Anal. Biochem.*, vol. 301, no. 2, pp. 261–277, Feb. 2002.
[24] R. Badugu, E. Descrovi, and J. R. Lakowicz, “Radiative decay engineering 7: Tamm state-coupled emission using a hybrid plasmonic-photonic structure.,” *Anal. Biochem.*, vol. 445, pp. 1–13, Jan. 2014.
[25] T. Ming, H. Chen, R. Jiang, Q. Li, and J. Wang, “Plasmon-Controlled Fluorescence: Beyond the Intensity Enhancement,” *J. Phys. Chem. Lett.*, vol. 3, no. 2, pp. 191–202, Jan. 2012.
[26] W. Srituravanich, N. Fang, C. Sun, Q. Luo, and X. Zhang, “Plasmonic Nanolithography,” *Nano Lett.*, vol. 4, no. 6, pp. 1085–1088, Jun. 2004.
[27] A. N. Grigorenko, N. W. Roberts, M. R. Dickinson, and Y. Zhang, “Nanometric optical tweezers based on nanostructured substrates,” *Nat. Photonics*, vol. 2, no. 6, pp. 365–370, May 2008.
[28] Z. Kang, H. Zhang, H. Lu, J. Xu, H.-C. Ong, P. Shum, and H.-P. Ho, “Plasmonic optical trap having very large active volume realized with nano-ring structure.,” *Opt. Lett.*, vol. 37, no. 10, pp. 1748–50, May 2012.
[29] M. Ploschner, “Optical forces near a nanoantenna,” *J. Nanophotonics*, vol. 4, no. 1, p. 041570, Feb. 2010.
[30] K. Wang and K. B. Crozier, “Plasmonic trapping with a gold nanopillar.,” *Chemphyschem*, vol. 13, no. 11, pp. 2639–48, Aug. 2012.
[31] M. L. Juan, M. Righini, and R. Quidant, “Plasmon nano-optical tweezers,” *Nat. Photonics*, vol. 5, no. 6, pp. 349–356, Jun. 2011.
[32] K. Wang, E. Schonbrun, P. Steinvurzel, and K. B. Crozier, “Trapping and rotating nanoparticles using a plasmonic nano-tweezer with an integrated heat sink.,” *Nat. Commun.*, vol. 2, p. 469, Jan. 2011.
[33] H. a Atwater and A. Polman, “Plasmonics for improved photovoltaic devices.,” *Nat. Mater.*, vol. 9, no. 3, pp. 205–13, Mar. 2010.
[34] F. J. Beck, S. Mokkapati, and K. R. Catchpole, “Plasmonic light-trapping for Si solar cells using self-assembled, Ag nanoparticles,” *Prog. Photovoltaics Res. Appl.*, vol. 18, no. 7, pp. 500–504, Jul. 2010.
[35] K. R. Catchpole, S. Mokkapati, F. Beck, E. Wang, A. McKinley, A. Basch, and J. Lee, “Plasmonics and nanophotonics for photovoltaics,” *MRS Bull.*, vol. 36, no. 06, pp. 461–467, Jun. 2011.
[36] Y. Yang, S. Pillai, H. Mehrvarz, H. Kampwerth, a. Ho-Baillie, and M. a. Green, “Enhanced light trapping for high efficiency crystalline solar cells by the application of rear surface plasmons,” *Sol. Energy Mater. Sol. Cells*, vol. 101, pp. 217–226, Jun. 2012.

[37] C. Höppener and L. Novotny, “Exploiting the light-metal interaction for biomolecular sensing and imaging.,” *Q. Rev. Biophys.*, vol. 45, no. 2, pp. 209–55, May 2012.
[38] J. R. Lakowicz, “Plasmonics in Biology and Plasmon-Controlled Fluorescence.,” *Plasmonics*, vol. 1, no. 1, pp. 5–33, Mar. 2006.
[39] J. S. Yuk, M. Trnavsky, C. McDonagh, and B. D. MacCraith, “Surface plasmon-coupled emission (SPCE)-based immunoassay using a novel paraboloid array biochip.,” *Biosens. Bioelectron.*, vol. 25, no. 6, pp. 1344–9, Feb. 2010.
[40] K. Ray, M. H. Chowdhury, J. Zhang, Y. Fu, H. Szmacinski, K. Nowaczyk, and J. R. Lakowicz, “Plasmon-controlled fluorescence towards high-sensitivity optical sensing.,” *Adv. Biochem. Eng. Biotechnol.*, vol. 116, pp. 29–72, Jan. 2010.
[41] M. Trnavsky, “Surface plasmon-coupled emission for applications in biomedical diagnostics,” Dublin City University, 2009.
[42] P. Berini and I. De Leon, “Surface plasmon–polariton amplifiers and lasers,” *Nat. Photonics*, vol. 6, no. 1, pp. 16–24, Dec. 2011.
[43] M. a. Noginov, G. Zhu, M. Bahoura, J. Adegoke, C. Small, B. a. Ritzo, V. P. Drachev, and V. M. Shalaev, “The effect of gain and absorption on surface plasmons in metal nanoparticles,” *Appl. Phys. B*, vol. 86, no. 3, pp. 455–460, Aug. 2006.
[44] D. Bergman and M. Stockman, “Surface Plasmon Amplification by Stimulated Emission of Radiation: Quantum Generation of Coherent Surface Plasmons in Nanosystems,” *Phys. Rev. Lett.*, vol. 90, no. 2, p. 027402, Jan. 2003.
[45] M. I. Stockman, “Spaser Action, Loss Compensation, and Stability in Plasmonic Systems with Gain,” *Phys. Rev. Lett.*, vol. 106, no. 15, p. 156802, Apr. 2011.
[46] C. W. Thiel, “Energies of rare-earth ion states relative to host bands in optical materials from electron photoemission spectroscopy,” Montana State University, 2003.
[47] S. Pikker, L. Dolgov, S. Heinsalu, S. Mamykin, V. Kiisk, S. Kopanchuk, R. Lõhmus, and I. Sildos, “Gilded nanoparticles for plasmonically enhanced fluorescence in TiO2:Sm3+ sol-gel films.,” *Nanoscale Res. Lett.*, vol. 9, no. 1, p. 143, Jan. 2014.
[48] L. Dolgov, V. Kiisk, R. Matt, S. Pikker, and I. Sildos, “Tailoring of the spectral–directional characteristics of rare-earth fluorescence by metal–dielectric planar structures,” *Appl. Phys. B*, vol. 107, no. 3, pp. 749–753, May 2012.
[49] L. Dolgov, V. Reedo, V. Kiisk, S. Pikker, I. Sildos, and J. Kikas, “Structure and fluorescent properties of TiO2:Sm3+–Ag composite,” *Opt. Mater. (Amst).*, vol. 32, no. 11, pp. 1540–1544, Sep. 2010.
[50] L. Dolgov, V. Kiisk, V. Reedo, S. Pikker, I. Sildos, and J. Kikas, “Sensitizing of Sm3+ fluorescence by silver dopant in the TiO2 films,” *Cent. Eur. J. Phys.*, vol. 9, no. 2, pp. 542–546, Oct. 2010.
[51] L. Dolgov, V. Kiisk, V. Reedo, A. Maaroos, I. Sildos, and J. Kikas, “Sol-gel derived metal oxides doped with silver nanoparticles as tunable plasmonic materials,” *Phys. Status Solidi A*, vol. 207, no. 5, pp. 1166–1169, Apr. 2010.
[52] V. Kiisk, V. Reedo, M. Karbowiak, M. G. Brik, and I. Sildos, “Spectroscopic and crystal field study of Sm 3+ in different phases of TiO 2,” *J. Phys. D. Appl. Phys.*, vol. 42, no. 12, p. 125107, Jun. 2009.
[53] A. M. Zaitsev, *Optical Properties of Diamond*. Berlin, Heidelberg: Springer Berlin Heidelberg, 2001.

[54] R. Mildren and J. Rabeau, *Optical Engineering of Diamond*. Weinheim, Germany: Wiley-VCH Verlag GmbH & Co. KGaA, 2013.
[55] B. J. M. Hausmann, B. Shields, Q. Quan, P. Maletinsky, M. McCutcheon, J. T. Choy, T. M. Babinec, A. Kubanek, A. Yacoby, M. D. Lukin, and M. Loncar, "Integrated diamond networks for quantum nanophotonics.," *Nano Lett.*, vol. 12, no. 3, pp. 1578–82, Mar. 2012.
[56] N. B. Manson and J. P. Harrison, "Photo-ionization of the nitrogen-vacancy center in diamond," *Diam. Relat. Mater.*, vol. 14, no. 10, pp. 1705–1710, Oct. 2005.
[57] Y. Dumeige, F. Treussart, R. Alléaume, T. Gacoin, J.-F. Roch, and P. Grangier, "Photo-induced creation of nitrogen-related color centers in diamond nanocrystals under femtosecond illumination," *J. Lumin.*, vol. 109, no. 2, pp. 61–67, Aug. 2004.
[58] T. Gaebel, M. Domhan, C. Wittmann, I. Popa, F. Jelezko, J. Rabeau, A. Greentree, S. Prawer, E. Trajkov, P. R. Hemmer, and J. Wrachtrup, "Photo-chromism in single nitrogen-vacancy defect in diamond," *Appl. Phys. B*, vol. 82, no. 2, pp. 243–246, Nov. 2005.
[59] D. Zheng, "Study and manipulation of photoluminescent NV color center in diamond," East China Normal University, 2010.
[60] L. Novotny and B. Hecht, *Principles of Nano-Optics*. Cambridge: Cambridge University Press, 2006.
[61] W. L. Barnes, "Fluorescence near interfaces: The role of photonic mode density," *J. Mod. Opt.*, vol. 45, no. 4, pp. 661–699, Apr. 1998.
[62] P. Anger, P. Bharadwaj, and L. Novotny, "Enhancement and Quenching of Single-Molecule Fluorescence," *Phys. Rev. Lett.*, vol. 96, no. 11, p. 113002, Mar. 2006.
[63] R. M. Amos and W. L. Barnes, "Modification of the spontaneous emission rate of Eu3+ ions close to a thin metal mirror," *Phys. Rev. B*, vol. 55, no. 11, pp. 7249–7254, Mar. 1997.
[64] W. H. Weber and C. F. Eagen, "Energy transfer from an excited dye molecule to the surface plasmons of an adjacent metal," *Opt. Lett.*, vol. 4, no. 8, p. 236, Aug. 1979.
[65] E. J. AMBROSE, "A Surface Contact Microscope for the study of Cell Movements," *Nature*, vol. 178, no. 4543, pp. 1194–1194, Nov. 1956.
[66] D. Axelrod, "Cell-substrate contacts illuminated by total internal reflection fluorescence.," *J. Cell Biol.*, vol. 89, no. 1, pp. 141–5, Apr. 1981.
[67] J. Enderlein, T. Ruckstuhl, and S. Seeger, "Highly efficient optical detection of surface-generated fluorescence.," *Appl. Opt.*, vol. 38, no. 4, pp. 724–32, Feb. 1999.
[68] T. Ruckstuhl and D. Verdes, "Supercritical angle fluorescence (SAF) microscopy.," *Opt. Express*, vol. 12, no. 18, pp. 4246–54, Sep. 2004.
[69] T. Liebermann and W. Knoll, "Surface-plasmon field-enhanced fluorescence spectroscopy," *Colloids Surfaces A Physicochem. Eng. Asp.*, vol. 171, no. 1–3, pp. 115–130, Oct. 2000.
[70] F. Stefani, K. Vasilev, N. Bocchio, N. Stoyanova, and M. Kreiter, "Surface-Plasmon-Mediated Single-Molecule Fluorescence Through a Thin Metallic Film," *Phys. Rev. Lett.*, vol. 94, no. 2, p. 023005, Jan. 2005.

[71] K. Ray, H. Szmacinski, J. Enderlein, and J. R. Lakowicz, “Distance dependence of surface plasmon-coupled emission observed using Langmuir-Blodgett films.,” *Appl. Phys. Lett.*, vol. 90, no. 25, p. 251116, Jun. 2007.
[72] J. R. Lakowicz, J. Malicka, I. Gryczynski, and Z. Gryczynski, “Directional surface plasmon-coupled emission: a new method for high sensitivity detection,” *Biochem. Biophys. Res. Commun.*, vol. 307, no. 3, pp. 435–439, Aug. 2003.
[73] E. Kretschmann and H. Raether, “Radiative decay of nonradiative surface plasmons excited by light,” *Z. Naturforsch. A*, vol. 23, p. 2135, 1968.
[74] S.-H. Cao, W.-P. Cai, Q. Liu, and Y.-Q. Li, “Surface plasmon-coupled emission: what can directional fluorescence bring to the analytical sciences?,” *Annu. Rev. Anal. Chem. (Palo Alto. Calif).*, vol. 5, pp. 317–36, Jan. 2012.
[75] D. G. Zhang, X.-C. Yuan, A. Bouhelier, P. Wang, and H. Ming, “Excitation of surface plasmon polaritons guided mode by Rhodamine B molecules doped in a PMMA stripe.,” *Opt. Lett.*, vol. 35, no. 3, pp. 408–10, Feb. 2010.
[76] D. G. Zhang, X.-C. Yuan, G. H. Yuan, P. Wang, and H. Ming, “Directional fluorescence emission characterized with leakage radiation microscopy,” *J. Opt.*, vol. 12, no. 3, p. 035002, Mar. 2010.
[77] K. H. Drexhage, “Influence of a dielectric interface on fluorescence decay time,” *J. Lumin.*, vol. 1–2, pp. 693–701, Jan. 1970.
[78] S. Kumar, A. Huck, Y. Chen, and U. L. Andersen, “Coupling of a single quantum emitter to end-to-end aligned silver nanowires,” *Appl. Phys. Lett.*, vol. 102, no. 10, p. 103106, 2013.
[79] A. B. Tesler, B. M. Maoz, Y. Feldman, A. Vaskevich, and I. Rubinstein, “Solid-State Thermal Dewetting of Just-Percolated Gold Films Evaporated on Glass: Development of the Morphology and Optical Properties,” *J. Phys. Chem. C*, vol. 117, no. 21, pp. 11337–11346, May 2013.
[80] M. T. Zin, K. Leong, N.-Y. Wong, H. Ma, M. Sarikaya, and A. K.-Y. Jen, “Surface-plasmon-enhanced fluorescence from periodic quantum dot arrays through distance control using biomolecular linkers.,” *Nanotechnology*, vol. 20, no. 1, p. 15305, Jan. 2009.
[81] K. Ray and J. R. Lakowicz, “Metal-Enhanced Fluorescence Lifetime Imaging and Spectroscopy on a Modified SERS Substrate,” *J. Phys. Chem. C*, vol. 117, no. 30, pp. 15790–15797, 2013.
[82] G. Liu and B. Jacquier, *Spectroscopic properties of rare earths in optical materials*, vol. 83. Berlin, Heidelberg: Springer-Verlag, 2005.
[83] V. Kiisk, M. Šavel, V. Reedo, A. Lukner, and I. Sildos, “Anatase-to-rutile phase transition of samarium-doped powder detected via the luminescence of,” *Phys. Procedia*, vol. 2, no. 2, pp. 527–538, Aug. 2009.
[84] W. Xue-Wei, W. Da-Jian, and L. Xiao-Jun, “Silver-Doping Induced Lattice Distortion in TiO 2 Nanoparticles,” *Chinese Phys. Lett.*, vol. 26, no. 7, p. 077809, Jul. 2009.
[85] T. Ohsaka, F. Izumi, and Y. Fujiki, “Raman spectrum of anatase, TiO2,” *J. Raman Spectrosc.*, vol. 7, no. 6, pp. 321–324, Dec. 1978.
[86] G. A. Tompsett, G. A. Bowmaker, R. P. Cooney, J. B. Metson, K. A. Rodgers, and J. M. Seakins, “The Raman spectrum of brookite, TiO2 (Pbca, Z = 8),” *J. Raman Spectrosc.*, vol. 26, no. 1, pp. 57–62, Jan. 1995.
[87] G. V. Krylova, Y. I. Gnatyuk, N. P. Smirnova, a. M. Eremenko, and V. M. Gun’ko, “Ag nanoparticles deposited onto silica, titania, and zirconia

mesoporous films synthesized by sol–gel template method," *J. Sol-Gel Sci. Technol.*, vol. 50, no. 2, pp. 216–228, Mar. 2009.

[88] G. E. Malashkevich, a. V. Semchenko, a. a. Sukhodola, a. P. Stupak, a. V. Sukhodolov, B. V. Plyushch, V. V. Sidskiĭ, and G. a. Denisenko, "Influence of silver on the Sm3+ luminescence in 'Aerosil' silica glasses," *Phys. Solid State*, vol. 50, no. 8, pp. 1464–1472, Aug. 2008.

[89] M. Elisa, I. Cristina Vasiliu, C. E. A. Grigorescu, B. Grigoras, H. Niciu, D. Niciu, A. Meghea, N. Iftimie, M. Giurginca, H. J. Trodahl, and M. Dalley, "Optical and structural investigation on rare-earth-doped aluminophosphate glasses," *Opt. Mater. (Amst).*, vol. 28, no. 6–7, pp. 621–625, May 2006.

[90] R. Swanepoel, "Determination of the thickness and optical constants of amorphous silicon," *J. Phys. E.*, vol. 16, no. 12, pp. 1214–1222, Dec. 1983.

[91] T. Ming, L. Zhao, Z. Yang, H. Chen, L. Sun, J. Wang, and C. Yan, "Strong polarization dependence of plasmon-enhanced fluorescence on single gold nanorods.," *Nano Lett.*, vol. 9, no. 11, pp. 3896–903, Nov. 2009.

[92] K. Tanaka, E. Plum, J. Y. Ou, T. Uchino, and N. I. Zheludev, "Multifold Enhancement of Quantum Dot Luminescence in Plasmonic Metamaterials," *Phys. Rev. Lett.*, vol. 105, no. 22, p. 227403, Nov. 2010.

[93] L. Zhao, T. Ming, H. Chen, Y. Liang, and J. Wang, "Plasmon-induced modulation of the emission spectra of the fluorescent molecules near gold nanorods.," *Nanoscale*, vol. 3, no. 9, pp. 3849–59, Sep. 2011.

[94] M. Ringler, a. Schwemer, M. Wunderlich, a. Nichtl, K. Kürzinger, T. Klar, and J. Feldmann, "Shaping Emission Spectra of Fluorescent Molecules with Single Plasmonic Nanoresonators," *Phys. Rev. Lett.*, vol. 100, no. 20, p. 203002, May 2008.

[95] E. C. LeRu, P. Etchegoin, J. Grand, N. Felidj, J. Aubard, and G. Levi, "Mechanisms of Spectral Profile Modification in Surface-Enhanced Fluorescence," *J. Phys. Chem. C*, vol. 111, no. 44, pp. 16076–16079, Nov. 2007.

[96] F. Birembaut, N. Perney, K. Pechstedt, P. N. Bartlett, A. E. Russell, and J. J. Baumberg, "Sharp-cornered liquid drops by wetting of nanoscale features.," *Small*, vol. 4, no. 12, pp. 2140–2, Dec. 2008.

[97] N. Perney, F. García de Abajo, J. Baumberg, A. Tang, M. Netti, M. Charlton, and M. Zoorob, "Tuning localized plasmon cavities for optimized surface-enhanced Raman scattering," *Phys. Rev. B*, vol. 76, no. 3, p. 035426, Jul. 2007.

[98] T. Teperik and A. Borisov, "Optical resonances in the scattering of light from a nanostructured metal surface: A three-dimensional numerical study," *Phys. Rev. B*, vol. 79, no. 24, p. 245409, Jun. 2009.

[99] N. M. B. Perney, J. J. Baumberg, M. E. Zoorob, M. D. B. Charlton, S. Mahnkopf, and C. M. Netti, "Tuning localized plasmons in nanostructured substrates for surface-enhanced Raman scattering," *Opt. Express*, vol. 14, no. 2, pp. 847–857, Jan. 2006.

ACKNOWLEDGEMENTS

I would like to express my sincere gratitude to everyone who has helped and supported me throughout my studies.

Above all I want to thank my supervisors Rünno Lõhmus, Ilmo Sildos, and Leonid Dolgov for their infinite support and guidance. I am also thankful to my former supervisors Raivo Stern from National Institute of Chemical Physics and Biophysics, Paul Leiderer from University of Konstanz and Girsh Blumberg from Rutgers University for all their help and advice during my studies.

I am sincerely grateful to all my colleagues at the Institute of Physics (especially Valter Kiisk, Vladimir Hižnjakov, Mihkel Rähn, Ardi Loot, Taavi Repän, Tanel Tätte, Meeri Visnapuu, Erik Randla) who have been a great joy to work with. I am also very thankful to Sergei Kopantšuk, Ago Rinken, and Lauri Sikk for the pleasant cooperation.

I would also like to express my gratitude to my opponent Prof. Gintautas Tamulaitis for taking the time and analysing my work and for the critical discussion.

Thank you KFV!

I am deeply indebted to my family and my dear Anni for their endless and invaluable love, support and patience.

This work was supported by Estonian Science Foundation (grants no 6999, Estonian Nanotechnology Competence Center (EU29996), ERDF projects (3.2.1101.12-0027, 3.2.1101.12-0028, 3.2.1101.12-0010, "Mesosystems: Theory and Applications" TK114), Estonian Research Council (target-financed theme IUT2-25) and has also been partially supported by graduate school "Functional materials and technologies", receiving funding from the European Social Fund under project 1.2.0401.09-0079 in Estonia.

PUBLICATIONS

CURRICULUM VITAE

Name:	Siim Pikker
Date of birth:	27.06.1984, Võru, Estonia
Citizenship:	Estonian
Address:	Institute of Physics, University of Tartu Ravila 14 50411 Tartu
Telephone:	+372 505 9521
E-mail:	siim.pikker@ut.ee

Education:

2009–2014	University of Tartu, Ph.D. student in physics
2012–2012	Rutgers, The State University of New Jersey, visiting researcher
2006–2009	University of Tartu, M.Sc. (applied physics, nanotechnology)
2007–2008	University of Konstanz, exchange student (Herbert-Quandt-Stiftung scholarship)
2003–2006	University of Tartu, B.Sc. (physics)
2000–2003	Hugo Treffner Gymnasium
1991–2000	Kreutzwald Gymnasium

Language skills: Estonian, English, German

Professional employment:

2011–	University of Tartu, Institute of Physics; engineer
2010–2011	University of Tartu, Institute of Physics; specialist
2008–2012	Estonian Nanotechnology Competence Center; engineer
2008–2009	University of Tartu, Institute of Physics; engineer
2006–2006	Estonian Nanotechnology Competence Center; lab assistant
2005–2005	Estonian Physical Society, lecturer

Awards

2012	Award for supervising student Ardi Loot who received I prize at the Estonian national student research competition
2009	The Student Scholarship of Institute of Physics, University of Tartu
2007	The scholarship of Herbert-Quandt-Stiftung

Dissertations supervised:

2014	Ardi Loot, M.Sc. “Enhancement of Spontaneous Emission by Plasmon Effects” (University of Tartu)
2014	Taavi Repän, M.Sc. “Sub-wavelength imaging with hyperbolic metamaterials” (University of Tartu)

List of publications

[1] S. Pikker, L. Dolgov, S. Heinsalu, S. Mamykin, V. Kiisk, S. Kopanchuk, R. Lõhmus, and I. Sildos, "Gilded nanoparticles for plasmonically enhanced fluorescence in TiO2:Sm3+ sol-gel films.," *Nanoscale Res. Lett.*, vol. 9, no. 1, p. 143, Jan. 2014.

[2] I. Oja Acik, L. Dolgov, M. Krunks, A. Mere, V. Mikli, S. Pikker, A. Loot, and I. Sildos, "Surface plasmon resonance caused by gold nanoparticles formed on sprayed TiO2 films," *Thin Solid Films*, vol. 553, pp. 144–147, Feb. 2014.

[3] T. Repän, S. Pikker, L. Dolgov, A. Loot, J. Hiie, M. Krunks, and I. Sildos, "Increased Efficiency inside the CdTe Solar Cell Absorber Caused by Plasmonic Metal Nanoparticles," *Energy Procedia*, vol. 44, pp. 229–233, 2014.

[4] A. Loot, L. Dolgov, and S. Pikker, "Goniometric Setup for Plasmonic Measurements and Characterization of Optical Coatings," in *Nano-materials Imaging Techniques, Surface Studies, and Applications*, Part II., O. Fesenko, L. Yatsenko, and M. Brodin, Eds. Springer New York, 2013, pp. 119–134.

[5] L. Dolgov, V. Kiisk, R. Matt, S. Pikker, and I. Sildos, "Tailoring of the spectral–directional characteristics of rare-earth fluorescence by metal–dielectric planar structures," *Appl. Phys. B*, vol. 107, no. 3, pp. 749–753, May 2012.

[6] L. Dolgov, V. Kiisk, S. Pikker, A. Loot, and I. Sildos, "Fluorescence of TiO 2 :Sm 3+ composite stimulated by plasmon waves," *IOP Conf. Ser. Mater. Sci. Eng.*, vol. 38, p. 012006, Aug. 2012.

[7] V. Kiisk, T. Kangur, M. Paalo, T. Tätte, S. Lange, S. Pikker, and I. Sildos, "Structural and luminescence characteristics of SnO2:Eu and SnO2:Eu,Sb nanophosphors upon annealing at high temperatures," *Mater. Chem. Phys.*, vol. 130, no. 1–2, pp. 293–298, Oct. 2011.

[8] V. Kiisk, T. Kangur, M. Paalo, T. Tätte, S. Pikker, and I. Sildos, "Optical characterization of sol-gel-derived SnO2:Eu nanopowders annealed at high temperatures," *Phys. status solidi*, vol. 8, no. 9, pp. 2641–2644, Sep. 2011.

[9] L. Dolgov, V. Kiisk, V. Reedo, S. Pikker, I. Sildos, and J. Kikas, "Sensitizing of Sm3+ fluorescence by silver dopant in the TiO2 films," *Cent. Eur. J. Phys.*, vol. 9, no. 2, pp. 542–546, Oct. 2010.

[10] L. Dolgov, V. Reedo, V. Kiisk, S. Pikker, I. Sildos, and J. Kikas, "Structure and fluorescent properties of TiO2:Sm3+–Ag composite," *Opt. Mater. (Amst).*, vol. 32, no. 11, pp. 1540–1544, Sep. 2010.

[11] L. A. Kommel, V. Mikli, R. Traksmaa, M. Saarna, A. Pokatilov, S. Pikker, and I. Kommel, "Influence of the SPD Processing Features on the Nanostructure and Properties of a Pure Niobium," *Mater. Sci. Forum*, vol. 667–669, pp. 785–790, Dec. 2010.

ELULOOKIRJELDUS

Nimi:	Siim Pikker
Sünniaeg:	27. juuni 1984, Võru
Kodakondsus:	Eesti
Kontaktandmed:	Tartu Ülikooli Füüsika Instituut Ravila 14 50411 Tartu
Telefon:	+3725059521
E-post:	siim.pikker@ut.ee

Haridustee:

2009–2014	Tartu Ülikool, doktorantuur (füüsika)
2012–2012	Rutgersi Ülikool, külalisuurija
2006–2009	Tartu Ülikool, MSc (rakendusfüüsika, nanotehnoloogia)
2007–2008	Konstanzi Ülikool, külalisüliõpilane Herbert-Quandt-Stiftungi stipendiaadina
2003–2006	Tartu Ülikool, BSc (füüsika)
2000–2003	Hugo Treffneri Gümnaasium
1991–2000	Võru Kreutzwaldi Gümnaasium

Keeleoskus: eesti keel, inglise keel**,** saksa keel

Teenistuskäik

2011–	Tartu Ülikool, Füüsika Instituut; insener
2010–2011	Tartu Ülikool, Füüsika Instituut; spetsialist
2008–2012	AS Eesti Nanotehnoloogiate Arenduskeskus; insener
2008–2009	Tartu Ülikool, Füüsika Instituut; insener
2006–2006	Eesti Nanotehnoloogiate Arenduskeskuse AS; laborant
2005–2005	Eesti Füüsika Selts, lektor

Tunnustused

2012	Tänukiri üliõpilaste teadustööde riiklikul konkursil I preemia pälvinud teadustöö juhendajale Ardi Loodi bakalaureusetöö „Pinnaplasmonite ja kullakile karakteriseerimine Kretschmanni skeemiga" juhendamise eest
2009	Tartu Ülikooli Füüsika Instituudi üliõpilasstipendium
2007	Herbert-Quandt-Stiftungi stipendium

Juhendamisel kaitstud väitekirjad

2014	Ardi Loot, magistritöö „Spontaanse kiirguse võimendamine plasmonefektide abil" (Tartu Ülikool)
2014	Taavi Repän, magistritöö „Sub-wavelength imaging with hyperbolic metamaterials" (Tartu Ülikool)

Publikatsioonide loetelu

[1] S. Pikker, L. Dolgov, S. Heinsalu, S. Mamykin, V. Kiisk, S. Kopanchuk, R. Lõhmus, and I. Sildos, "Gilded nanoparticles for plasmonically enhanced fluorescence in TiO2:Sm3+ sol-gel films.," *Nanoscale Res. Lett.*, vol. 9, no. 1, p. 143, Jan. 2014.

[2] I. Oja Acik, L. Dolgov, M. Krunks, A. Mere, V. Mikli, S. Pikker, A. Loot, and I. Sildos, "Surface plasmon resonance caused by gold nanoparticles formed on sprayed TiO2 films," *Thin Solid Films*, vol. 553, pp. 144–147, Feb. 2014.

[3] T. Repän, S. Pikker, L. Dolgov, A. Loot, J. Hiie, M. Krunks, and I. Sildos, "Increased Efficiency inside the CdTe Solar Cell Absorber Caused by Plasmonic Metal Nanoparticles," *Energy Procedia*, vol. 44, pp. 229–233, 2014.

[4] A. Loot, L. Dolgov, and S. Pikker, "Goniometric Setup for Plasmonic Measurements and Characterization of Optical Coatings," in *Nanomaterials Imaging Techniques, Surface Studies, and Applications*, Part II., O. Fesenko, L. Yatsenko, and M. Brodin, Eds. Springer New York, 2013, pp. 119–134.

[5] L. Dolgov, V. Kiisk, R. Matt, S. Pikker, and I. Sildos, "Tailoring of the spectral–directional characteristics of rare-earth fluorescence by metal–dielectric planar structures," *Appl. Phys. B*, vol. 107, no. 3, pp. 749–753, May 2012.

[6] L. Dolgov, V. Kiisk, S. Pikker, A. Loot, and I. Sildos, "Fluorescence of TiO 2 :Sm 3+ composite stimulated by plasmon waves," *IOP Conf. Ser. Mater. Sci. Eng.*, vol. 38, p. 012006, Aug. 2012.

[7] V. Kiisk, T. Kangur, M. Paalo, T. Tätte, S. Lange, S. Pikker, and I. Sildos, "Structural and luminescence characteristics of SnO2:Eu and SnO2:Eu,Sb nanophosphors upon annealing at high temperatures," *Mater. Chem. Phys.*, vol. 130, no. 1–2, pp. 293–298, Oct. 2011.

[8] V. Kiisk, T. Kangur, M. Paalo, T. Tätte, S. Pikker, and I. Sildos, "Optical characterization of sol-gel-derived SnO2:Eu nanopowders annealed at high temperatures," *Phys. status solidi*, vol. 8, no. 9, pp. 2641–2644, Sep. 2011.

[9] L. Dolgov, V. Kiisk, V. Reedo, S. Pikker, I. Sildos, and J. Kikas, "Sensitizing of Sm3+ fluorescence by silver dopant in the TiO2 films," *Cent. Eur. J. Phys.*, vol. 9, no. 2, pp. 542–546, Oct. 2010.

[10] L. Dolgov, V. Reedo, V. Kiisk, S. Pikker, I. Sildos, and J. Kikas, "Structure and fluorescent properties of TiO2:Sm3+–Ag composite," *Opt. Mater. (Amst).*, vol. 32, no. 11, pp. 1540–1544, Sep. 2010.

[11] L. A. Kommel, V. Mikli, R. Traksmaa, M. Saarna, A. Pokatilov, S. Pikker, and I. Kommel, "Influence of the SPD Processing Features on the Nanostructure and Properties of a Pure Niobium," *Mater. Sci. Forum*, vol. 667–669, pp. 785–790, Dec. 2010.

DISSERTATIONES PHYSICAE UNIVERSITATIS TARTUENSIS

1. **Andrus Ausmees.** XUV-induced electron emission and electron-phonon interaction in alkali halides. Tartu, 1991.
2. **Heiki Sõnajalg.** Shaping and recalling of light pulses by optical elements based on spectral hole burning. Tartu, 1991.
3. **Sergei Savihhin.** Ultrafast dynamics of F-centers and bound excitons from picosecond spectroscopy data. Tartu, 1991.
4. **Ergo Nõmmiste.** Leelishalogeniidide röntgenelektronemissioon kiiritamisel footonitega energiaga 70–140 eV. Tartu, 1991.
5. **Margus Rätsep.** Spectral gratings and their relaxation in some low-temperature impurity-doped glasses and chrystals. Tartu, 1991.
6. **Tõnu Pullerits.** Primary energy transfer in photosynthesis. Model calculations. Tartu, 1991.
7. **Olev Saks.** Attoampri diapasoonis voolude mõõtmise füüsikalised alused. Tartu, 1991.
8. **Andres Virro.** AlGaAsSb/GaSb heterostructure injection lasers. Tartu, 1991.
9. **Hans Korge.** Investigation of negative point discharge in pure nitrogen at atmospheric pressure. Tartu, 1992.
10. **Jüri Maksimov.** Nonlinear generation of laser VUV radiation for high-resolution spectroscopy. Tartu, 1992.
11. **Mark Aizengendler.** Photostimulated transformation of aggregate defects and spectral hole burning in a neutron-irradiated sapphire. Tartu, 1992.
12. **Hele Siimon.** Atomic layer molecular beam epitaxy of A^2B^6 compounds described on the basis of kinetic equations model. Tartu, 1992.
13. **Tõnu Reinot.** The kinetics of polariton luminescence, energy transfer and relaxation in anthracene. Tartu, 1992.
14. **Toomas Rõõm.** Paramagnetic H^{2-} and F^+ centers in CaO crystals: spectra, relaxation and recombination luminescence. Tallinn, 1993.
15. **Erko Jalviste.** Laser spectroscopy of some jet-cooled organic molecules. Tartu, 1993.
16. **Alvo Aabloo.** Studies of crystalline celluloses using potential energy calculations. Tartu, 1994.
17. **Peeter Paris.** Initiation of corona pulses. Tartu, 1994.
18. **Павел Рубин.** Локальные дефектные состояния в CuO_2 плоскостях высокотемпературных сверхпроводников. Тарту, 1994.
19. **Olavi Ollikainen.** Applications of persistent spectral hole burning in ultrafast optical neural networks, time-resolved spectroscopy and holographic interferometry. Tartu, 1996.
20. **Ülo Mets.** Methodological aspects of fluorescence correlation spectroscopy. Tartu, 1996.
21. **Mikhail Danilkin.** Interaction of intrinsic and impurity defects in CaS:Eu luminophors. Tartu, 1997.

22. **Ирина Кудрявцева.** Создание и стабилизация дефектов в кристаллах KBr, KCl, RbCl при облучении ВУФ-радиацией. Тарту, 1997.
23. **Andres Osvet.** Photochromic properties of radiation-induced defects in diamond. Tartu, 1998.
24. **Jüri Örd.** Classical and quantum aspects of geodesic multiplication. Tartu, 1998.
25. **Priit Sarv.** High resolution solid-state NMR studies of zeolites. Tartu, 1998.
26. **Сергей Долгов.** Электронные возбуждения и дефектообразование в некоторых оксидах металлов. Тарту, 1998.
27. **Kaupo Kukli.** Atomic layer deposition of artificially structured dielectric materials. Tartu, 1999.
28. **Ivo Heinmaa.** Nuclear resonance studies of local structure in $RBa_2Cu_3O_{6+x}$ compounds. Tartu, 1999.
29. **Aleksander Shelkan.** Hole states in CuO_2 planes of high temperature superconducting materials. Tartu, 1999.
30. **Dmitri Nevedrov.** Nonlinear effects in quantum lattices. Tartu, 1999.
31. **Rein Ruus.** Collapse of 3d (4f) orbitals in 2p (3d) excited configurations and its effect on the x-ray and electron spectra. Tartu, 1999.
32. **Valter Zazubovich.** Local relaxation in incommensurate and glassy solids studied by Spectral Hole Burning. Tartu, 1999.
33. **Indrek Reimand.** Picosecond dynamics of optical excitations in GaAs and other excitonic systems. Tartu, 2000.
34. **Vladimir Babin.** Spectroscopy of exciton states in some halide macro- and nanocrystals. Tartu, 2001.
35. **Toomas Plank.** Positive corona at combined DC and AC voltage. Tartu, 2001.
36. **Kristjan Leiger.** Pressure-induced effects in inhomogeneous spectra of doped solids. Tartu, 2002.
37. **Helle Kaasik.** Nonperturbative theory of multiphonon vibrational relaxation and nonradiative transitions. Tartu, 2002.
38. **Tõnu Laas.** Propagation of waves in curved spacetimes. Tartu, 2002.
39. **Rünno Lõhmus.** Application of novel hybrid methods in SPM studies of nanostructural materials. Tartu, 2002.
40. **Kaido Reivelt.** Optical implementation of propagation-invariant pulsed free-space wave fields. Tartu, 2003.
41. **Heiki Kasemägi.** The effect of nanoparticle additives on lithium-ion mobility in a polymer electrolyte. Tartu, 2003.
42. **Villu Repän.** Low current mode of negative corona. Tartu, 2004.
43. **Алексей Котлов.** Оксианионные диэлектрические кристаллы: зонная структура и электронные возбуждения. Tartu, 2004.
44. **Jaak Talts.** Continuous non-invasive blood pressure measurement: comparative and methodological studies of the differential servo-oscillometric method. Tartu, 2004.
45. **Margus Saal.** Studies of pre-big bang and braneworld cosmology. Tartu, 2004.

46. **Eduard Gerškevitš.** Dose to bone marrow and leukaemia risk in external beam radiotherapy of prostate cancer. Tartu, 2005.
47. **Sergey Shchemelyov.** Sum-frequency generation and multiphoton ionization in xenon under excitation by conical laser beams. Tartu, 2006.
48. **Valter Kiisk.** Optical investigation of metal-oxide thin films. Tartu, 2006.
49. **Jaan Aarik.** Atomic layer deposition of titanium, zirconium and hafnium dioxides: growth mechanisms and properties of thin films. Tartu, 2007.
50. **Astrid Rekker.** Colored-noise-controlled anomalous transport and phase transitions in complex systems. Tartu, 2007.
51. **Andres Punning.** Electromechanical characterization of ionic polymer-metal composite sensing actuators. Tartu, 2007.
52. **Indrek Jõgi.** Conduction mechanisms in thin atomic layer deposited films containing TiO_2. Tartu, 2007.
53. **Aleksei Krasnikov.** Luminescence and defects creation processes in lead tungstate crystals. Tartu, 2007.
54. **Küllike Rägo.** Superconducting properties of MgB_2 in a scenario with intra- and interband pairing channels. Tartu, 2008.
55. **Els Heinsalu.** Normal and anomalously slow diffusion under external fields. Tartu, 2008.
56. **Kuno Kooser.** Soft x-ray induced radiative and nonradiative core-hole decay processes in thin films and solids. Tartu, 2008.
57. **Vadim Boltrushko.** Theory of vibronic transitions with strong nonlinear vibronic interaction in solids. Tartu, 2008.
58. **Andi Hektor.** Neutrino Physics beyond the Standard Model. Tartu, 2008.
59. **Raavo Josepson.** Photoinduced field-assisted electron emission into gases. Tartu, 2008.
60. **Martti Pärs.** Study of spontaneous and photoinduced processes in molecular solids using high-resolution optical spectroscopy. Tartu, 2008.
61. **Kristjan Kannike.** Implications of neutrino masses. Tartu, 2008.
62. **Vigen Issahhanjan.** Hole and interstitial centres in radiation-resistant MgO single crystals. Tartu, 2008.
63. **Veera Krasnenko.** Computational modeling of fluorescent proteins. Tartu, 2008.
64. **Mait Müntel.** Detection of doubly charged higgs boson in the CMS detector. Tartu, 2008.
65. **Kalle Kepler.** Optimisation of patient doses and image quality in diagnostic radiology. Tartu, 2009.
66. **Jüri Raud.** Study of negative glow and positive column regions of capillary HF discharge. Tartu, 2009.
67. **Sven Lange.** Spectroscopic and phase-stabilisation properties of pure and rare-earth ions activated ZrO_2 and HfO_2. Tartu, 2010.
68. **Aarne Kasikov.** Optical characterization of inhomogeneous thin films. Tartu, 2010.

69. **Heli Valtna-Lukner.** Superluminally propagating localized optical pulses. Tartu, 2010.
70. **Artjom Vargunin.** Stochastic and deterministic features of ordering in the systems with a phase transition. Tartu, 2010.
71. **Hannes Liivat.** Probing new physics in e+e− annihilations into heavy particles via spin orientation effects. Tartu, 2010.
72. **Tanel Mullari.** On the second order relativistic deviation equation and its applications. Tartu, 2010.
73. **Aleksandr Lissovski.** Pulsed high-pressure discharge in argon: spectroscopic diagnostics, modeling and development. Tartu, 2010.
74. **Aile Tamm.** Atomic layer deposition of high-permittivity insulators from cyclopentadienyl-based precursors. Tartu, 2010.
75. **Janek Uin.** Electrical separation for generating standard aerosols in a wide particle size range. Tartu, 2011.
76. **Svetlana Ganina.** Hajusandmetega ülesanded kui üks võimalus füüsikaõppe efektiivsuse tõstmiseks. Tartu, 2011
77. **Joel Kuusk.** Measurement of top-of-canopy spectral reflectance of forests for developing vegetation radiative transfer models. Tartu, 2011.
78. **Raul Rammula**. Atomic layer deposition of HfO_2 – nucleation, growth and structure development of thin films. Tartu, 2011.
79. **Сергей Наконечный.** Исследование электронно-дырочных и интерстициал-вакансионных процессов в монокристаллах MgO и LiF методами термоактивационной спектроскопии. Тарту, 2011.
80. **Niina Voropajeva.** Elementary excitations near the boundary of a strongly correlated crystal. Tartu, 2011.
81. **Martin Timusk.** Development and characterization of hybrid electro-optical materials. Tartu, 2012, 106 p.
82. **Merle Lust.** Assessment of dose components to Estonian population. Tartu, 2012, 84 p.
83. **Karl Kruusamäe.** Deformation-dependent electrode impedance of ionic electromechanically active polymers. Tartu, 2012, 128 p.
84. **Liis Rebane.** Measurement of the $W \to \tau\nu$ cross section and a search for a doubly charged Higgs boson decaying to τ-leptons with the CMS detector. Tartu, 2012, 156 p.
85. **Jevgeni Šablonin.** Processes of structural defect creation in pure and doped MgO and NaCl single crystals under condition of low or super high density of electronic excitations. Tartu, 2013, 145 p.
86. **Riho Vendt**. Combined method for establishment and dissemination of the international temperature scale. Tartu, 2013, 108 p.
87. **Peeter Piksarv.** Spatiotemporal characterization of diffractive and non-diffractive light pulses. Tartu, 2013, 156 p.
88. **Anna Šugai.** Creation of structural defects under superhigh-dense irradiation of wide-gap metal oxides. Tartu, 2013, 108 p.

89. **Ivar Kuusik.** Soft X-ray spectroscopy of insulators. Tartu, 2013, 113 p.
90. **Viktor Vabson**. Measurement uncertainty in Estonian Standard Laboratory for Mass. Tartu, 2013, 134 p.
91. **Kaupo Voormansik.** X-band synthetic aperture radar applications for environmental monitoring. Tartu, 2014, 117 p.
92. **Deivid Pugal.** hp-FEM model of IPMC deformation. Tartu, 2014, 143 p.